

Projecting end of century climate extremes and their impacts on the hydrology of a representative California watershed

Fadji Z. Maina^{1,3*}, Alan Rhoades², Erica R. Siirila-Woodburn¹, Peter-James Denny-Frank¹

¹ Energy Geosciences Division, Lawrence Berkeley National Laboratory 1 Cyclotron Road, M.S. 74R-316C, Berkeley, CA 94704, USA

² Climate and Ecosystem Sciences Division, Lawrence Berkeley National Laboratory 1 Cyclotron Road, M.S. 74R-316C, Berkeley, CA 94704, USA

³ now at NASA Goddard Space Flight Center, Hydrological Sciences Laboratory, Greenbelt, MD, USA

*Corresponding Author: fadjizaouna.maina@nasa.gov

Abstract

In California, it is essential to understand the evolution of water resources in response to a changing climate to sustain its economy and agriculture and to build resilient communities. Although extreme conditions have characterized the historical hydroclimate of California, climate change will likely intensify hydroclimatic extremes by the End of Century (EoC). However, few studies have investigated the impacts of EoC extremes on watershed hydrology. We use cutting-edge global climate and integrated hydrologic models to simulate EoC extremes and their effects on the water-energy balance. We assess the impacts of projected driest, median, and wettest water years under a Representative Concentration Pathway (RCP) 8.5 on the hydrodynamics of the Cosumnes river basin. Substantial changes to annual average temperature ($>+2.5^{\circ}\text{C}$) and precipitation ($>+38\%$) will characterize the EoC extreme water years compared to their historical counterparts. A shift in the dominant form of precipitation, mostly in the form of rain, is projected to fall earlier. These changes reduce snowpack by more than 90%, increase peak surface water and groundwater storages up to 75% and 23%, respectively, and drive the timing of peak storage to occur earlier in the year. Because EoC temperatures and soil moisture are high, both potential and actual evapotranspiration (*ET*) increase. The latter, along with the lack of snowmelt in the warm EoC, cause surface water and groundwater storages to significantly decrease in summer, with groundwater showing the highest rates of decrease. These changes result in more ephemeral EoC streams with more focused flow and increased storage in the mainstem of the river network during the summer.

Keywords: future climate extremes, integrated hydrologic model, global climate model, end of century hydrology, watershed hydrology, water management

Introduction

California, the fifth-largest economy in the world, hosts one of the largest agricultural regions in the United States and is home to over 39 million people. Because of its geographic location, Mediterranean climate, geology, and landscape, the state of California is sensitive to climate change (Hayhoe et al. 2004). Understanding how water resources will evolve under a changing climate is crucial for sustaining the state's economy and agricultural productivity. The region is especially susceptible to climate change given its reliance on the Sierra Nevada mountain snowpack as a source of water supply (e.g., Dettinger & Anderson, 2015). Studies show that temperatures may warm by as much as 4.5°C by the End of Century (hereafter, EoC) (Cayan et al., 2008), that snowpack is expected to decrease as most precipitation will fall as rain instead of snow (Rhoades et al., 2018a,b; Siirila-Woodburn, et al., 2021), and that rain on snow events will exacerbate melt (Cayan et al., 2008; Gleick, 1987; Maurer, 2007; Mote et al., 2005; Musselman, Clark, et al., 2017; Musselman, Molotch, et al., 2017). Given that precipitation falls predominantly in winter months and the summers are hot and dry, the snow accumulated during the winter provides important water storage for the dry season and is crucial to meet urban demand, sustain ecosystem function, and maintain agricultural productivity (Bales et al., 2006; Dierauer et al., 2018). As such, any significant reduction in the snowpack has the potential to drastically affect the hydrology of the state (Barnett et al., 2005; Harpold & Molotch, 2015; Milly et al., 2005; Rhoades et al., 2018 a,b).

Over the past several decades, researchers have worked to understand how changes in Sierra Nevada snowpack will affect important hydrologic fluxes such as evapotranspiration (Tague & Peng, 2013) and streamflow (Berghuijs et al., 2014; Gleick, 1987; He et al., 2019; Maurer, 2007; Safeeq et al., 2014; Son & Tague, 2019; Vicuna & Dracup, 2007; Vicuna et al., 2007). For

example, analyses of recent historical trends show that snowpack reductions result in increases in winter streamflow and decreases in summer streamflow (e.g. Safeeq et al., 2012). However, the sensitivity of a given area to these climatic changes depends on many factors including geology and therefore drainage efficiency, topography, and land cover (Alo & Wang, 2008; Christensen et al., 2008; Cristea et al., 2014; Ficklin et al., 2013; Mayer & Naman, 2011; Safeeq et al., 2015; Son & Tague, 2019; Tang et al., 2019).

Climate change in California is also expected to lead to unprecedented extreme conditions, which include severe drought and intense deluge (Swain et al., 2018). In recent years, these changes have already been observed in the forms of multi-year droughts (Cook et al., 2004; Griffin & Anchukaitis, 2014; Shukla et al., 2015) and high-intensity precipitation events mainly caused by atmospheric rivers (Dettinger et al., 2004; Dettinger, 2011; Dettinger, 2013; Ralph & Dettinger, 2011; Ralph et al., 2006). These unprecedented conditions will require water management strategies to adapt to ensure demands are met. This will be especially true if periods of precipitation become more extreme, variable, and occur over a shorter window of time (Swain et al., 2018; Gershunov et al., 2019; Huang et al., 2020; Rhoades et al., 2020b; Rhoades et al., 2021).

To project how changes in climate will impact watershed behavior, high-resolution, physics-based models are needed to simulate system dynamics accurately, particularly those that are non-linear, and constitute a better way to analyze a no-analog future. Previous studies analyzed future hydrologic conditions in California but relied on models that do not 1) account for the interactions, feedbacks, and movements of water from the lower atmosphere to the subsurface; 2) represent groundwater dynamics and lateral flow; 3) incorporate physics-based high-resolution climate models and/or 4) hydrologic models (e.g., Berghuijs et al., 2014; Gleick, 1987; He et al., 2019; Maurer, 2007; Safeeq et al., 2014; Son & Tague, 2019; Vicuna & Dracup, 2007; Vicuna et

al., 2007). Considerations of coupled interactions that explicitly account for groundwater connections are important (Condon et al., 2020, 2013; Maxwell and Condon, 2016). Also, previous studies have focused on the mid-century period (e.g., Maurer & Duffy, 2005; Son & Tague, 2019), which may indicate a more muted signal in hydrologic impacts than at EoC. Understanding these impacts is essential because long-term climate projections show that extremes will become more frequent and intense by the EoC (Cayan et al., 2008).

In this work, we assess the impacts of EoC extremely dry and intensely wet conditions on the hydrodynamics of a Californian watershed that contains one of the last naturally flowing rivers in the state. This allows us to investigate the impacts of climate change without the complexity of active water management, and thus to set the context for water management decisions. We specifically investigate how the water-energy balance responds to climate change, and how those changes propagate to alter the spatiotemporal distribution of water in different hydrologic compartments of the watershed. We focus our investigation on the changes in groundwater and surface water storages. The balance of these two natural reservoirs, and their relationship in response to changes in snowpack changes, is important for water management decision making. We aim to 1) strengthen our physics-based understanding of the main hydrologic processes controlling changes in water storages under a changing climate, 2) quantify the magnitude and timing of these shifts in storage, and 3) identify the areas that are most vulnerable to change. To do so, we utilize a novel combination of cutting-edge climate and hydrologic model simulations. We drive the integrated hydrologic model Parflow-CLM (ParFlow-CLM; Maxwell & Miller, 2005) with climate forcing from a physics-based, variable-resolution enabled global climate model (the Variable Resolution enabled Community Earth System Model, VR-CESM; Zarzycki et al., 2014) that dynamically couples multi-scale interactions within the atmosphere-ocean-land system.

1. Study Area: The Cosumnes watershed

The Cosumnes River is one of the last rivers in the western United States without a major dam, offering a rare opportunity to isolate the impacts of a changing climate on the hydrodynamics without reservoir management consideration (Maina et al., 2020a; Maina and Siirila-Woodburn, 2020). The watershed spans the Central Valley-Sierra Nevada interface and therefore represents important aspects of the large-scale hydrology patterns of the state, namely the assessment of interactions between changes in precipitation, snowpack, streamflow, and groundwater across elevation and geologic gradients. Located in Northern California, USA, the Cosumnes watershed is approximately 7,000 km² in size (Figure 1) and is situated between the American and the Mokelumne rivers. Its geology ranges from low-permeability rocks typical of the Sierra Nevada landscape (volcanic and plutonic) to the porous and permeable alluvial depositions of the Central Valley aquifers. These are separated by very low-permeability marine sediments. The watershed topography includes a range of landscapes typical of the region (e.g. varying from flat agricultural land, rolling foothills, and steep mountainous hillsides), and elevation varies from approximately 2500 m in the upper watershed to sea level in the Central Valley (Figure 1). The Sierra Nevada mountains are characterized by evergreen forest while the Central Valley hosts an intensive agricultural region including crops such as alfalfa, vineyards, as well as pastureland. Like other Californian watersheds, the climate in the Cosumnes is Mediterranean consisting of wet and cold winters (with a watershed average temperature equal to 0°C) and hot and dry summers (with watershed average temperature reaching 25°C) (Cosgrove et al., 2003).

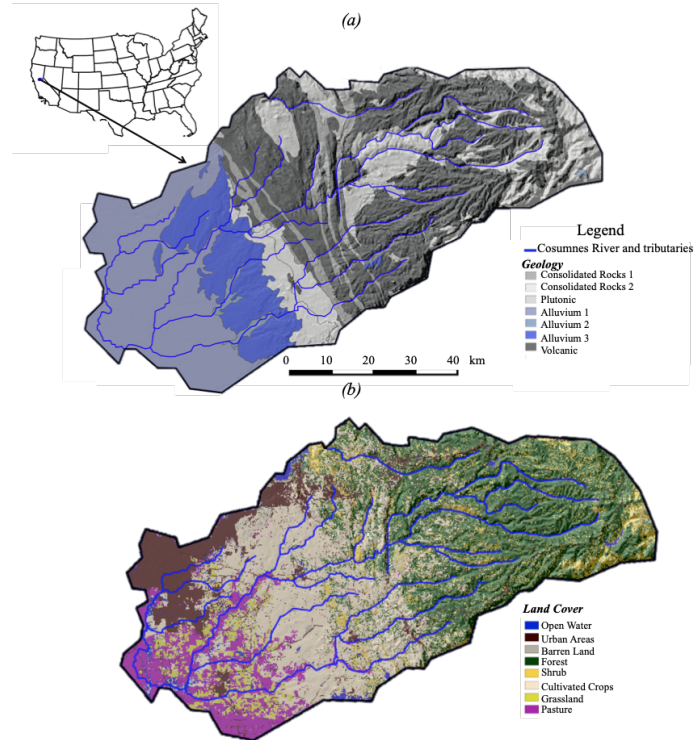


Figure 1: The Cosumnes Watershed (a) location and geology (Jennings et al., 1977), the alluvium in blue corresponds to the Central Valley aquifers whereas the consolidated rocks in gray correspond to the Sierra Nevada and cross-cutting marine sediments, and (b) land cover (Homer et al., 2015).

2. Modeling Framework

2.1. Variable Resolution Community Earth System Model (VR-CESM)

Our modeling approach represents both dynamical and thermodynamic atmospheric response to climate change across scales, different from “pseudo-global warming” and “statistical delta” approaches used in many hydrologic modeling studies. While these approaches are useful to isolate the impact of a given perturbation and/or variable, expected changes in climate will involve the co-evolution of many processes, and may therefore not account for compensating factors. The interaction between dynamical and thermodynamic responses has important, and

sometimes, offsetting effects on features such as atmospheric rivers. For example, Payne et al. (2020) show that the thermodynamic response to climate change enhances atmospheric river characteristics (e.g., Clausius-Clapeyron relationship), whereas the dynamical response diminishes atmospheric river characteristics (e.g., changes in the jet stream and storm track landfall location). Therefore, VR-CESM may simulate a more inclusive hydroclimatic response to climate change in the western United States at a resolution that is at the cutting-edge of today's global climate modeling capabilities for decadal-to-centennial length simulations (Haarsma et al., 2016). Historical and EoC meteorological forcings are obtained from a simulation using the VR-CESM at a regionally refined resolution of 28 km over the Northern Pacific Ocean through the western United States, including the Cosumnes watershed and a global resolution of 111 km. CESM has been jointly developed by NCAR (National Center for Atmospheric Research) and the DOE (U.S. Department of Energy) and simulates a continuum of Earth system processes including the atmosphere, land surface, land ice, ocean, ocean waves, and sea ice and the interactions between them (Collins et al., 2006; Gent et al., 2011; Hurrell et al., 2013). VR-CESM is a novel tool to perform dynamical downscaling as it allows for the interactions between the major components of the global climate system (e.g., atmosphere, cryosphere, land surface, and ocean) while allowing for regional-scale phenomena to emerge where regional refinement is applied, all within a single model (Huang et al., 2016; Rhoades et al., 2016; Rhoades, Ullrich, & Zarzycki, 2018b; Rhoades, Ullrich, Zarzycki, et al., 2018c).

The atmospheric model used for these simulations is the Community Atmosphere Model (CAM) version 5.4 with the spectral element dynamical core, with an atmospheric dynamics time step of 75 seconds, an atmospheric physics time step of 450 seconds, a prognostic treatment of rainfall and snowfall in the microphysics scheme (Gettelman and Morrison, 2015) and run under

Atmosphere Model Intercomparison Project (AMIP) protocols (Gates, 1992). Under the AMIP protocols, the atmosphere and land-surface components of the Earth system model are coupled and periodically bounded by monthly observed sea-surface temperatures and sea-ice extents. Although this configuration does not exactly recreate historical water years and events, it is expected to reasonably simulate the distribution of water year types (see Appendix A for more details). Also, it should be noted that the model only projects one scenario (RCP8.5) of future conditions with assumptions of greenhouse gas emissions, sea-surface temperatures, and sea ice extents and would not be expected to exactly forecast future water years, but rather an envelope of plausible future conditions. Simulations with VR-CESM are performed for 30-year periods based on the climates from a historical period (1985-2015) and an EoC period (2070-2100). EoC simulations, analogous to Rhoades, Ullrich, & Zarzycki, 2018, are bounded by estimates of future changes in ocean conditions derived from a fully-coupled bias-corrected CESM simulation and forced by greenhouse gases and aerosol concentrations assumed in the RCP8.5 emissions scenario. Historical VR-CESM outputs have been compared with reanalyses and future VR-CESM outputs have been analyzed for shifts in hydrometeorological extremes in Rhoades et al., 2020 a,b. To couple the outputs with ParFlow-CLM, we regrid the unstructured 28km VR-CESM data over the Cosumnes watershed using bilinear interpolation using the Earth System Modeling Framework (Jones, 1999) to a final resolution of approximately 11 km (i.e., 57 grid cells over the Cosumnes watershed). Notably, each of the spectral elements in the VR-CESM grid, shown in Figure A1, has a 4x4 set of Gauss–Lobatto–Legendre (GLL) quadrature nodes where equations of the atmospheric model are solved (Herrington et al., 2019). Therefore, the actual resolution at which the atmospheric dynamics and physics are solved in VR-CESM are at high-resolution (~28km), making these some of the highest resolution global Earth system model simulations over California

to date (Haarsma et al., 2016). VR-CESM simulations were evaluated by comparing them to a widely used observational product, the Parameter-elevation Relationships on Independent Slopes Model (PRISM; Daly et al., 2008) at 4 km resolution analogous to Rhoades et al., (2020a). More details about the comparisons can be found in Appendix A.

2.2. Integrated Hydrologic Model: ParFlow-CLM

The integrated hydrologic model ParFlow-CLM (Kollet & Maxwell, 2006; Maxwell, 2013; Maxwell & Miller, 2005) solves the transfer and interactions of water and energy from the subsurface to the lower atmosphere including groundwater dynamics, streamflow, infiltration, recharge, evapotranspiration, and snow dynamics. The model describes 3D groundwater flow in variably saturated media with the Richards equation (equation 1, Richards, 1931) and 2D overland flow with the kinematic wave equation (equation 2).

$$S_S S_W(\psi_P) \frac{\partial \psi_P}{\partial t} + \phi \frac{\partial S_W(\psi_P)}{\partial t} = \nabla \cdot [K(x) k_r(\psi_P) \nabla(\psi_P - z)] + q_s \quad (1)$$

Where is S_S the specific storage (L^{-1}), $S_W(\psi_P)$ is the degree of saturation (-) associated with the subsurface pressure head ψ_P (L), t is the time (T), ϕ is the porosity (-), k_r is the relative permeability (-), z is the depth, q_s is the source/sink term (T^{-1}) and $K(x)$ is the saturated hydraulic conductivity ($L T^{-1}$).

ParFlow solves the mixed form of the Richards equation which has the advantage of conserving the mass (Celia et al., 1990).

The kinematic wave equation is used to describe surface flow in two dimensions is defined as:

$$-k(x) k_r(\psi_0) \nabla(\psi_0 - z) = \frac{\partial \|\psi_0, 0\|}{\partial t} - \nabla \cdot \vec{v} \|\psi_0, 0\| - q_r(x) \quad (2)$$

Where ψ_0 is the ponding depth, $\|\psi_0, 0\|$ indicates the greater term between ψ_0 and 0, \vec{v} is the depth averaged velocity vector of surface runoff ($L T^{-1}$), q_r is a source/sink term representing rainfall and evaporative fluxes ($L T^{-1}$).

Surface water velocity at the surface in x and y directions, (v_x) and (v_y) respectively, is computed using the following set of equations:

$$v_x = \frac{\sqrt{S_{f,x}}}{m} \psi_0^{\frac{2}{3}} \text{ and } v_y = \frac{\sqrt{S_{f,y}}}{m} \psi_0^{\frac{2}{3}} \quad (3)$$

Where $S_{f,x}$ and $S_{f,y}$ friction slopes along x and y respectively and m is the Manning's coefficient. ParFlow employs a cell-centered finite difference scheme along with an implicit backward Euler scheme and the Newton Krylow linearization method to solve these nonlinear equations. The computational grid follows the terrain to mimic the slope of the domain (Maxwell, 2013).

ParFlow has many advantages in comparisons to other hydrologic models such as MODFLOW (Harbaugh, 2005), FEFLOW (Trefry and Muffels, 2007), SWAT (Soil and Water Assessment Tool) (Neitsch et al., 2000), and SAC-MA (Sacramento Soil Moisture Accounting Model). ParFlow's advantages include land surface processes such as snow dynamics and evapotranspiration and their interactions with the subsurface which are crucial for studying the hydrology of California. ParFlow also solves subsurface flow by accounting for variably saturated conditions, an important feature for calculating groundwater recharge and the connection between the groundwater and the land surface processes, which is not the case for the aforementioned models. While some hydrologic models have a better representation of the land surface processes such as Noah-MP (Niu et al., 2011) and VIC (Variable Infiltration Capacity Model Macroscale Hydrologic Model; Liang et al., 1994), these models do not have a detailed representation of the subsurface flows. Compared to other integrated hydrologic models including CATHY (Catchment Hydrology; Bixio et al., 2002) and MIKE-SHE (Abbott et al., 1986)), ParFlow has the advantage

that it solves a two-dimensional kinematic flow equation that is fully coupled to the Richards equation.

ParFlow is coupled to the Community Land Model (CLM) that solves the surface energy and water balance, which enables interactions between the land surface and the lower atmosphere and the calculation of key land surface processes governing the system hydrodynamics such as evapotranspiration, infiltration, and snow dynamics. CLM simulates the thermal processes by closing the energy balance at the land surface given by:

$$R_n(\theta) = LE(\theta) + H(\theta) + G(\theta) \quad (4)$$

Where $\theta = \phi S_w$ is the soil moisture, R_n is the net radiation at the land surface (E/LT) a balance between the shortwave (also called solar) and longwave radiation, LE is the latent heat flux (E/LT) which captures the energy required to change the phase of water, H is the sensible heat flux (E/LT) and G is the ground heat flux (E/LT).

More information about the coupling between ParFlow and CLM can be found in Maxwell & Miller, (2005). CLM uses the following forcings from the VR-CESM model at 3-hourly resolution to solve the energy balance at the land surface: precipitation, air temperature, specific humidity, atmospheric pressure, north/south and east/west wind speed, and shortwave and longwave wave radiation.

We constructed a high-resolution model of the Cosumnes watershed with a horizontal discretization of 200 m and vertical discretization that varies from 10 cm at the land surface to 30 m at the bottom of the domain. The model has 8 layers, the first 4 layers represent the soil layers and the other four the deeper subsurface. The total thickness of the domain is 80 m to ensure appropriate representation of water table dynamics. Observed water table depths (as measured at several wells located in the Central Valley portion of the domain) can reach approximately 50 m

below the land surface (Maina et al., 2020a). The resulting model comprises approximately 1.4 million active cells and was solved using 320 cores in a high-performance computing environment. The Cosumnes watershed is bounded by the American and Mokelumne rivers. We, therefore, impose weekly varying values of Dirichlet boundary conditions along these borders to reflect the observed changes of river stages. The eastern part of the watershed corresponding to the upper limit in the Sierra Nevada is modeled as a no-flow (i.e., Neumann) boundary condition. Hydrodynamic parameters required to solve the surface and subsurface flows (e.g., hydraulic conductivity, specific storage, porosity, and van Genuchten parameters) are derived from a regional geological map (Geologic Map of California, 2015; Jennings et al., 1977) and a literature review of previous studies (Faunt et al., 2010; Faunt and Geological Survey (U.S.), 2009; Gilbert and Maxwell, 2017; Welch and Allen, 2014). We use the 2011 National Land Cover Database (NLCD) map (Homer et al., 2015) to define land use and land cover required by CLM. We further delineate specific croplands (notably alfalfa, vineyards, and pasture) in the Central Valley by using the agricultural maps provided by the National Agricultural Statistics Service (NASS) of the US Department of Agriculture's (USDA) Cropland Data Layer (CDL) (Boryan et al., 2011). Vegetation parameters are defined by the International Geosphere-Biosphere Programme (IGBP) database (IGBP, 2018). A complete description of the model parameterization can be found in Appendix B and more details are provided in Maina et al. (2020a). Model validation of groundwater levels, river stages, and land surface processes (evapotranspiration, soil moisture, and snow water equivalent) was performed over a period of three years that includes extremely dry and wet water years (Appendix C). The model has also been successfully used in recent investigations of post-wildfire and hydrometeorological extreme conditions and to assess the role of meteorological forcing scale on simulated watershed dynamics (Maina et al., 2020a,b;

Maina and Siirila-Woodburn, 2020c). Initial conditions for pressure-head were obtained by a spin-up procedure using the forcing of the historical median WY. We recursively simulated the historical median WY forcing until the differences of storage at the end of the WY were less than 1%, indicating convergence. This pressure head field is then used as the initial condition for each of the five WYs of interest (i.e., the EoC wet, EoC dry, historic wet, historic dry, EoC median). Though we acknowledge land cover alterations are expected to occur by the EoC (either naturally or anthropogenically), in this work we assume that the vegetation remains constant for both historical and EoC simulations for simplicity. Further, while the Central Valley of California hosts intensive agriculture that is reliant on groundwater pumping for irrigation, we didn't incorporate pumping and irrigation in our model configuration because groundwater pumping rates may substantially change in the future due to new demands, policies, regulations, and changes in land cover and land use and aim to provide an estimate of the natural hydrologic system response to climate change.

2.3. Analysis of EoC hydrodynamics

To investigate how the EoC climate extremes affect water storages, we investigate five hydrologic variables: SWE , ET , Pressure-head (ψ) distributions, and surface and subsurface water storage. Total groundwater (GW) storage is given by:

$$Storage_{GW} = \sum_{i=1}^{n_{GW}} \Delta x_i \times \Delta y_i \times \Delta z_i \times \psi_i \times \left(\frac{S_{s_i}}{\phi_i} \right) \quad (5)$$

where n_{GW} is the total number of subsurface saturated cells (-), Δx_i and Δy_i are cell discretizations along the x and y directions (L), Δz_i is the discretization along the vertical direction the cell (L), S_{s_i} is the specific storage associated with cell i , ψ_i the pressure-head, and ϕ_i is the porosity.

Total surface water (SW) storage which accounts for any water located at the land surface (i.e., any cell of the model with a pressure-head greater than 0) and includes river water or overland flow is calculated via:

$$Storage_{SW} = \sum_{i=1}^{n_{SW}} \Delta x_i \times \Delta y_i \times \psi_i \quad (6)$$

where n_{SW} is the total number of cells with surface water i.e., with surface ψ greater than 0 (-), and i indicates the cell.

We compare each EoC WY simulation to its corresponding historical WY counterpart and both the historical and EoC medians. Comparisons are shown as a percent change (PC) calculated using:

$$PC_{i,t} = \frac{X_{projection_{i,t}} - X_{baseline_{i,t}}}{X_{baseline_{i,t}}} \times 100 \quad (3)$$

where X is the model output (ET , SWE , or ψ) at a given point in space (i) at a time (t), *baseline* is the selected simulation (historical median, EoC median, or historical extreme), and *projection* represents the simulation obtained with the EoC extreme WYs (dry or wet).

3. Results

In this section, we present a subset of the outputs from VR-CESM (precipitation and temperature) to identify the extreme (dry and wet) and median WYs of interest. Changes in fluxes and storages over the course of each WY, as well as the spatial variability of these changes in two hydrologically important periods of the WY (peak flow and baseflow) are also shown.

3.1. Selection of the median, dry, and wet WYs

From the historical and EoC 30-year VR-CESM simulations we select the median, wettest, and driest WYs for comparison (see Figure 2a). Overall, the future WYs are ~30% wetter than the historical WYs (p-value ~0.006 for two-tailed t-test of equal average annual precipitation) in addition to being ~4.6°C warmer. Precipitation and temperature variances are mostly similar in the

historical and EoC simulations, though EoC minimum temperature may be more variable (p-value ~ 0.059 for two-tailed f-test of equal variance in minimum temperature). On average the timing for the start, length, and end of precipitation is similar, though EoC precipitation may be less variable in its start time (p-value ~ 0.053 for f-test of equal variance in days to reach 5th percentile of annual precipitation). In the climate model, there are no clear trends between the precipitation timing metrics and total amount of precipitation.

The EoC median WY is much wetter than its historical counterpart, with about ~ 250 mm/year more precipitation that begins approximately 1 week earlier and ends approximately 2 weeks earlier in the year. The EoC wettest WY is much wetter than the historical wettest WY (42% more precipitation) and consistent with theory outlined in Allan et al. (2020). The EoC wettest WY is 3.8°C warmer than the historical wettest WY and 4.6°C warmer than the historical median WY, as the historical median WY is one of the coolest years in the series. Precipitation occurs earlier in the EoC wet WY compared to the historical wet or median WYs, with the 5th percentile of precipitation occurring 12 days earlier in the EoC wettest WY than either the wettest or median historical WYs. The duration of the EoC wettest WY precipitation season (146 days) is between the historical wettest WY (133 days) and the historical median WY (155 days). The EoC dry WY is also much wetter than its historic counterpart; in fact, the EoC dry WY is wetter than the seven driest historical WYs of the 30-year historical ensemble. Simulation of 30 random draws from two identical normal distributions, repeated 100,000 times, finds that the lowest value in one is higher than the seven lowest values in the other only $\sim 1.1\%$ of the time (p-value ~ 0.011). This statistical test reveals that this VR-CESM simulation suggests that future dry years will be wetter than historical dry years. The EoC dry WY is only $\sim 2.5^{\circ}\text{C}$ warmer than the historical dry WY. The divergence in temperature is smaller for the comparison of EoC and historical WYs of the dry

extremes as opposed to the wet extremes because the historical dry WY is the second-warmest WY in the historical simulations, while the EoC dry WY is the third coolest in the EoC simulations. Precipitation in the EoC dry WY starts particularly early, with the 5th percentile of annual precipitation reached by mid-October. This is much earlier than either the dry or median historical WYs, which don't reach that percentile of precipitation until mid-to-late November. The historical dry WY also has a particularly short precipitation duration of only 97 days, while the EoC dry WY has a 163-day precipitation duration, more similar to the median historical WY duration of 155 days.

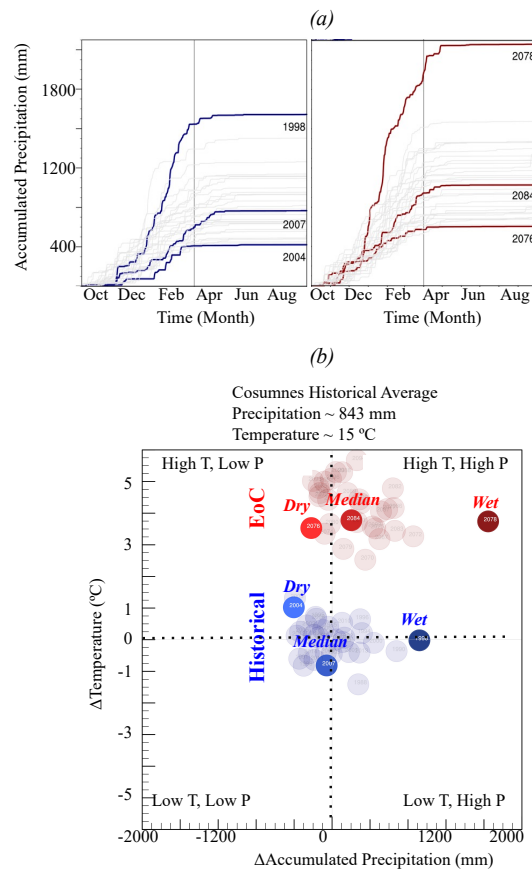


Figure 2: (a) VR-CESM accumulated total precipitation for the historical and End of Century (EoC) simulations, and (b) quadrants for differences between each individual water year (WY)

and the historical average temperature and accumulated precipitation in the Cosumnes watershed. The historical and EoC dry, median and wet WYs are indicated in blue and red, respectively.

Figure 3 shows the spatial distribution of accumulated precipitation anomalies across California. These anomalies are computed for each of the six identified WYs relative to the climatological average (the 30-year historical mean). These spatial plots provide context for the changes modeled in the Cosumnes watershed relative to broader precipitation changes California-wide. As in the Cosumnes, California-wide EoC dry, median, and wet WYs are all characterized by higher precipitation totals than their historical counterparts. Importantly, the EoC wet WY is a true outlier not only in the Cosumnes but across California too. Notably, California lies at an important large-scale circulation transition, namely semi-permanent high-pressure systems associated with the Hadley circulation. Therefore, how climate change alters the atmospheric dynamics over California, or more specifically how far northward storm-tracks may shift, remains uncertain and can depend on climate model choice. This has led to papers that claim the future of California will be wet across a range of climate models (e.g., Neelin et al, 2013; Swain et al., 2013; Gershunov et al., 2019; Rhoades et al., 2020b; Persad et al., 2020) and, for select climate models, that it could be drier. Notably, these studies highlight an asymmetric response in the frequency of wet versus dry WYs (i.e., anomalously wet WYs increase in frequency much more in the future than anomalously dry WYs). Many of the aforementioned studies also highlight that in anomalously wet WYs extreme precipitation events (e.g., atmospheric rivers) will occur with greater intensity and frequency and largely drive changes in WY precipitation totals (which is shown in our VR-CESM simulations for California in more detail in Rhoades et al., 2020b). Given these complexities and others such as consideration for how dynamical and thermodynamical

effects of climate change may interact with one another to offset or amplify extreme precipitation events (Payne et al., 2020), the hypothesis that global warming will result in a climate where the “wet gets wetter and dry gets drier” may be too simplistic of an assumption for California. Rhoades et al., (2020b) shows quantitatively that the increases in precipitation observed in the VR-CESM outputs are due to a greater number of intense atmospheric river events that occur more regularly back-to-back (recently corroborated by Rhoades et al. (2021) using uniform-high-resolution CESM simulations at different warming scenarios) and that atmospheric river precipitation totals increase at a much larger rate (+53%/K) than non-AR precipitation totals (+1.4%/K), which agrees with findings made in other studies such as Gershunov et al. (2019).

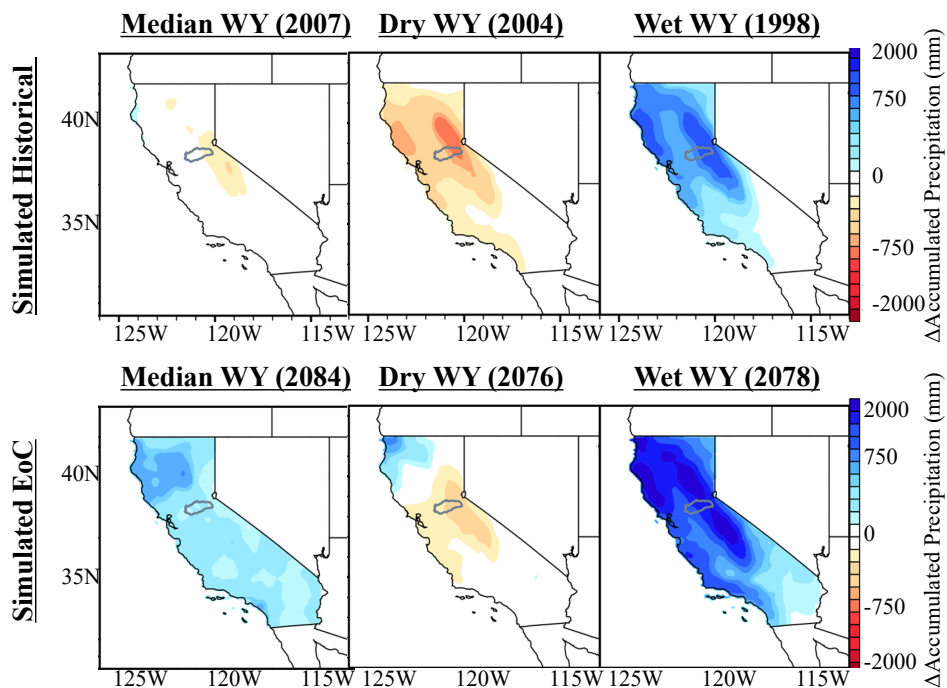


Figure 3: Precipitation spatial distributions of the dry, median, and wet water years (WY) for the 30-year historical and EoC simulations relative to the climatological average (derived from the 30-year historical mean)

3.2. Changes in annual watershed-integrated fluxes and storages

Figure 4 illustrates the annual changes in the integrated hydrologic budget of the Cosumnes watershed for the EoC WYs (i.e., median, dry, and wet) compared to the historical median WY. The EoC median WY compared to the historical median WY has 38% more precipitation and the temperature is 4.4°C higher. Further, the precipitation phase also shifts with an increase in rainfall (54%) and a decrease in snowfall (-54%). This results in a significant decrease in *SWE* (-91%) which is consistent with many other studies that have shown that increased temperatures due to climate change will lead to low-to-no snow conditions (Berghuijs et al., 2014; Cayan et al., 2008; Mote et al., 2005; Rhoades et al., 2018 a,b; Son & Tague, 2019; Siirila-Woodburn et al., 2021). The increase in temperature and precipitation results in an increase in *ET* (62%), consistent with the findings of other recent studies (e.g. McEvoy et al., 2020). Nevertheless, the larger amount of precipitation associated with the EoC is enough to offset higher *ET* demand and recharge groundwater and surface water, which increase by 4% and 19% respectively. The EoC wet WY has similar changes as the EoC median WY when compared to the historical wet WY yet the magnitude of the increase in surface (21%), and groundwater (11%) storages are higher due to more precipitation and higher temperatures. The dry EoC WY is also characterized by higher precipitation (43%, the largest increase) than its historical counterpart, this results in large increases in total groundwater (8%) and surface water (38%) storages.

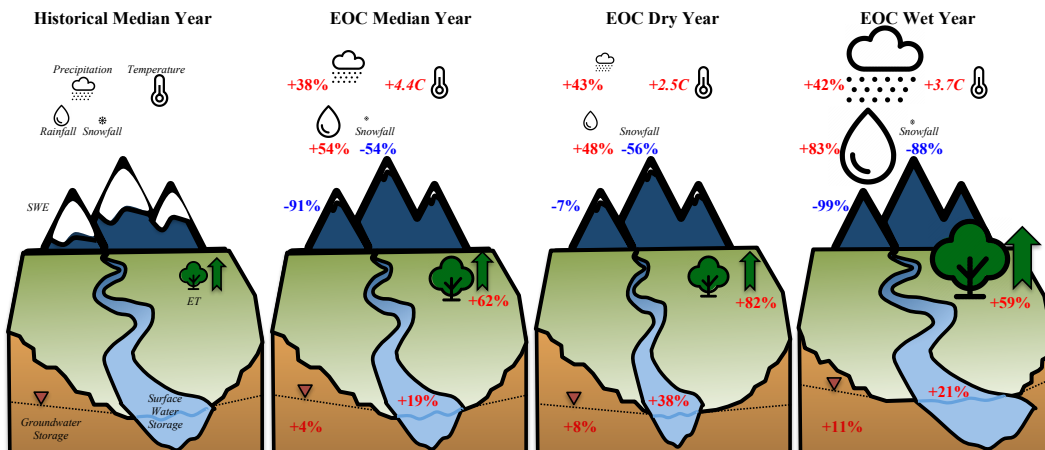


Figure 4: Annual percent changes in precipitation, rainfall, snowfall, temperature, *SWE*, *ET*, surface water, and groundwater storages in the EoC water years (WY) (i.e median, dry, and wet) at the watershed scale relative to their historical counterparts. Info-graphic size scaled to EoC conditions.

1.1. Temporal variation of watershed-integrated fluxes and storages

Understanding annual changes at the watershed scale is important to broadly understand changes in the water budget in response to future climate extremes. However, a deeper understanding of the processes that drive these changes and the interactions from atmosphere-through-bedrock requires an analysis of their spatiotemporal variations as well. Figure 5 shows the temporal variations of each of the historical and EoC WY's integrated hydrologic budgets grouped by WY type (columns), with a top-down sequencing of hydrologic variables of interest in order from the atmosphere through subsurface (rows). This organization allows for the investigation of propagating impacts to be directly compared in time. In this section, we discuss historical vs EoC changes observed in each of the WY types (i.e., median, dry, and wet). Each WY shows unique hydrodynamic behaviors and changes compared to the historical conditions. The median WY sheds light on how changes in the precipitation phase and increases in temperature and precipitation in the EoC will impact the hydrodynamics. The dry WYs allow comparing EoC and historical low-to-no snow conditions whereas assessing the hydrodynamics of the EoC wet WY provides a better understanding of how intense EoC precipitation along with the warm EoC climate will shape the hydrology.

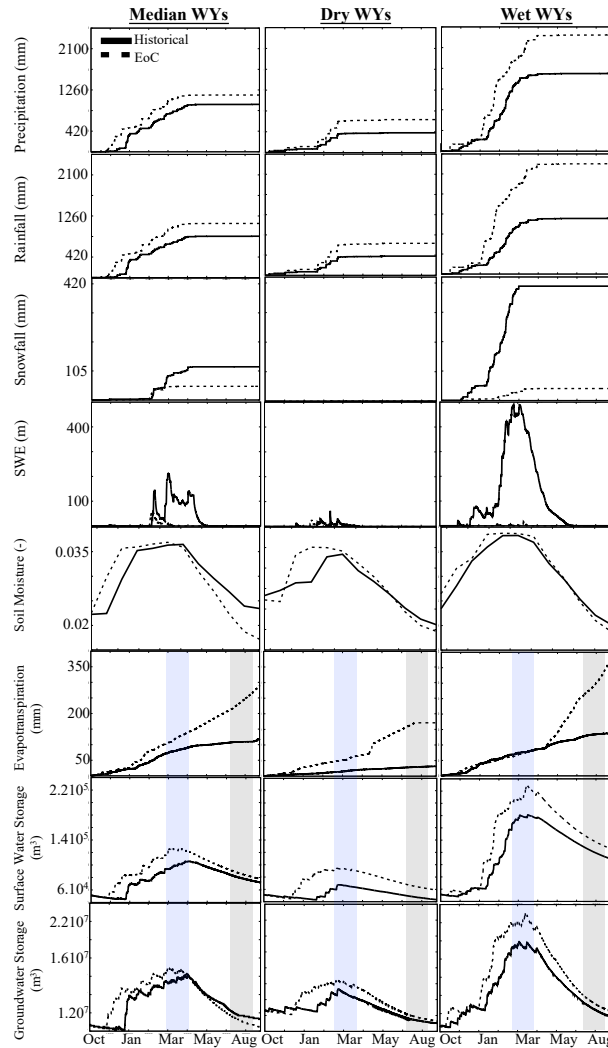


Figure 5: Temporal variations of the total cumulative precipitation, rainfall, and snowfall at the watershed scale, total *SWE* at the watershed scale, the average watershed values of soil moisture, the cumulative watershed *ET*, and the total surface water, and groundwater storages at the watershed scale associated with the six historical and EoC Water Years (WY). The blue area indicates the selected peak flow period while the gray area corresponds to the selected baseflow conditions for the spatial distribution analyses.

1.1.1. Median water years

As indicated in section 3.1, the EoC median WY has more precipitation than the historical median WY. The EoC precipitation comes mainly as rain due to the warmer temperatures of the

EoC and includes virtually no snowfall from late winter to early spring. This precipitation phase-change combined with the earlier snowfall cessation date in the WY results in minimal and even non-existent *SWE* in the Cosumnes watershed for much of the WY, a significant change compared to historic conditions. EoC peak *SWE* occurs in February in contrast to the historical peak *SWE*, which occurs in April. Due to the watershed's relatively low elevation, snow accumulates only in the upper part of the Cosumnes watershed (~10% of the total watershed area). Only areas located in the highest elevations (> 2000 m), such as the eastern limit of the watershed, show any *SWE* in the EoC simulations whereas in the historical WYs we observed *SWE* as low as 1000 m.

The decrease in snow and the increase in rain along with an earlier onset of seasonal precipitation directly impacts soil moisture, which sees an early increase with a slightly higher peak than historical. As more water is available earlier in the EoC, the *ET* demand from increased temperatures is met until substantially higher summer temperatures increase *ET* at a much faster rate than the historical WY. The high EoC *ET* and the lack of snowmelt cause the soil to rapidly dry from late-spring through late-summer.

Because of the marked increase in total precipitation and shift from snow to rain in the EoC simulations, surface water storage generally increases throughout the WY. This is consistent with previous studies (Gleick, 1987; He et al., 2019; Maurer, 2007; Safeeq et al., 2014; Son & Tague, 2019; Vicuna & Dracup, 2007; Vicuna et al., 2007). Surface water storage increases in early November in the EoC simulations while in the historical simulations this increase occurs in January. Similar to the earlier peak *SWE* and soil moisture, the peak surface water storage in the EoC is also earlier (January through February) compared to the historical period (March through April). This late-season surface water storage remains larger because the accumulated precipitation is large enough to overcome the increased *ET* in a warmer climate. Similar to surface water storage,

groundwater storage increases earlier and peaks at a larger amount than the historical WY. However, in contrast to the surface water storage, the groundwater storage during baseflow conditions is lower in the median EoC compared to the median historical year. This decrease in groundwater during baseflow conditions is due to the lack of snowmelt and higher EoC *ET*. In late spring and summer in the EoC, groundwater keeps depleting through *ET* and is not recharged by snowmelt through surface and subsurface flows from the Sierra Nevada as in the historical period. This may indicate that compared to surface water storage, groundwater storage may be more sensitive to EoC hydroclimatic changes (which are multi-fold, and in this case include an increase in precipitation, a transition from snow to rain, and higher *ET*). One way to quantitatively measure this sensitivity is to compare the seasonal change in water storage between peak and baseflow conditions. Historically, changes between peak and baseflow conditions (i.e., the amount of water lost between peak and base flow) resulted in moderate seasonal changes in groundwater storage (30%) and surface water storage (32%). The EoC simulations reveal larger seasonal variation for groundwater and surface water storage (40% and 37% decreases, respectively). Groundwater in the Cosumnes Watershed is mainly recharged in the headwaters and stored in the Central Valley. Therefore, these Central Valley aquifers experience earlier and larger increases in storage which lead to more water available for *ET* and therefore aquifer depletion. A deeper understanding of this phenomenon requires an analysis of the spatial patterns of these changes which is performed later on in this study.

1.1.2. Dry water years

All EoC WYs are characterized by higher precipitation in the form of rainfall compared to their historical counterparts. The historical dry WY has ~43% less total precipitation than the EoC dry WY. However, we note that for the EoC dry WY the decrease in snowfall is less drastic than

the median or wet EoC years. This is because the historically driest WY is significantly warmer than the historical average WY, and therefore already has a smaller snowpack, 94% lower than the historical median WY. The EoC dry WY *SWE* also accumulates two months earlier than the historical *SWE*. Because the differences in *SWE* between the dry WYs are smaller than the differences in *SWE* between the median WYs (7% versus 91%), we can deduce that the earlier and larger rise in soil moisture in the EoC dry WY is mostly due to an earlier and larger amount of rainfall. The higher soil moisture and EoC temperatures result in higher *ET* throughout the WY compared to the historical WY. This *ET* results in lower soil moisture by the end of the summer, similar to the median WY. In addition, surface water storage peaks earlier and at a larger amount compared to the historical WY. The surface water storage in the EoC remains higher throughout the WY compared to its historical counterpart despite this higher *ET* due to the low precipitation associated with the historical dry WY. We further note that the difference in surface water storage during baseflow conditions between the two dry WYs is higher than the difference between the two median WYs. The groundwater recharge starts two months earlier in the EoC driest WY compared to the historical driest WY due to the changes in timing and magnitude of precipitation. However, it is interesting to note that groundwater storage during baseflow conditions in the EoC WY is nearly equal to the historical WY (within 3%). Thus, although more water enters the EoC dry WY system through greater precipitation, it eventually exits by the end of the WY and no considerable net gains to groundwater are observed. This significant reduction in groundwater storage from late winter to end-of-summer is a result of the much larger EoC *ET* and highlights the dynamic nature of the EoC dry year watershed interactions. Also similar to the median WY, dry WY seasonal decreases in EoC storage are more pronounced in the groundwater signal (36%)

than in the surface water signal (33%). We further note that the decreases in groundwater and surface water storages are, as in the median WY, larger (+8%) than the historical decreases.

1.1.3. Wet water years

The EoC wet WY is significantly wetter than all other WYs. Yet, unlike the historical WY, the precipitation largely comes as rain, as shown by the low-to-no snowfall and *SWE* totals (Figure 5). The difference in future versus contemporary wet WY *SWE* (99%) is larger than the differences between the median and the dry WYs (91%). As in other WYs, soil moisture increases earlier compared to the historical wet WY. A greater water availability enables the system to meet the high EoC *ET* demand. Hence, *ET* in the EoC wettest year remains higher than the historical wettest year *ET* throughout the WY. However, the increase in *ET*, combined with the lack of snowmelt that can buffer and recharge soil moisture in spring, leads to less soil moisture at the end of the WY compared with the historical WY. Further, surface water storage increases earlier and at a much faster rate in the EoC WY compared to the historical WY. This is mirrored in the groundwater storages. As in the other EoC simulations, when compared to the historical counterpart the EoC wettest year shows a sharper decline in seasonal above and below groundwater storage changes (occurring between peak flow and baseflow). Groundwater storage decreases 47% in the EoC between peak flow and baseflow, whereas only a 41% decrease occurs in the historical wet WY. Similarly, surface water storage decreases 44% in the EoC whereas only a 41% decrease occurs in the historical wet WY.

1.2. Spatial patterns of the changes in fluxes and pressure-heads

1.2.1. Median water years

Figure 6 shows the percent changes in *ET*, surface water pressure-heads, and subsurface pressure-heads (i.e., pressure-heads of the model bottom layer) in the EoC median WY compared

to the historical median WY during peak flow and baseflow conditions (see the time frames in Figure 5). Regions in red correspond to areas with smaller fluxes or pressure-heads in the EoC compared to the historical ones, whereas regions in blue correspond to areas with larger fluxes or pressure-heads in the EoC compared to the historical median WY. We study peak flow and baseflow conditions because the analysis of the temporal variations of fluxes and storages has shown that these two periods are characterized by different trends and represent the key periods in understanding the hydrologic responses to the EoC extreme climate.

Relative to the historical median WY, during peak flow the EoC median WY is characterized by an increased *ET* across the majority of the watershed, especially in the Central Valley, and larger surface water and subsurface pressure-heads (Figure 6a-c). *ET* increases in the EoC both because of the increase in water availability and increased evaporative demand, as discussed in the previous section (3.3.1.). The increase in *ET* is non-uniform across the watershed because of the heterogeneity of the landscape's topographical gradients, land-surface cover, and subsurface geological conditions. The Central Valley is characterized by a large increase in *ET* compared to the Sierra Nevada, and the patterns of *ET* in the Central Valley are also more homogeneous, a resultant of the geological characteristics of the area and the hydroclimate of the watershed. This leads to more water available in the Central Valley compared to the Sierra Nevada characterized by less permeable rocks. In addition, as most of the *ET* in the Central Valley comes from evaporation due to the high temperatures of the EoC (not shown here), the increase in evaporation is higher in the Central Valley due to its aquifers characterized by a high permeability (Maina and Siirila-Woodburn, 2020) and the availability of water.

Surface and subsurface pressure heads both show general increases during the EoC peak flow, yet these maps reveal that unlike *ET* the pressure head (and therefore storage) of water is

very heterogeneous in space. For example, in the Sierra Nevada, we observe an increase in subsurface pressure-head (Figure 6c) only in some relatively permeable areas susceptible to infiltration and recharge. Although the Central Valley aquifers are more permeable and geologically less heterogeneous than the Sierra Nevada (as defined in the model), the changes in subsurface pressure-head in the Central Valley are heterogeneous. This is because the recharge of the Central Valley aquifers is dependent on the subsurface and surface flows from the headwater. Only areas of the Central Valley that are subject to stronger connectivity with the headwaters see an increase in subsurface pressure-head in the EoC.

Relative to its historical counterpart, the EoC median WY is characterized by high *ET* during baseflow conditions though less than during peak flow conditions. (Figure 6d). We observe larger surface water pressure-heads in higher-order streams whereas surface water pressure-heads decrease in the EoC in the majority of the low-order, ephemeral streams (Figure 6e). This opposition of spatial pattern trends, resulting in more water in the main river channels, and less in the smaller streams, occurs for several reasons. First, peak flow occurs earlier in the EoC and is more rainfed, so that the ephemeral streams drain earlier in the EoC compared to historical. This sustained and longer duration of drainage increases the surface water pressure-head along the main river channels and is due to the contribution of the subsurface flow from the headwaters. This contribution is also higher in the EoC due to larger amounts of precipitation. The trends along the main river channel are also evident in the subsurface pressure-head maps (Figure 6f). Because the surface water is larger along the main channels, the subsurface pressure-heads are also larger here due to the interconnection between the subsurface and the surface (Figure 6f). However, in general, subsurface pressure-heads decrease elsewhere in the EoC during baseflow because of the lack of snowmelt and the higher *ET* demand. This result highlights the spatiotemporal complexity of an

expected watershed's response to changes in climate (shown here to be bi-directional), and how factors such as river proximity may be crucial for consideration.

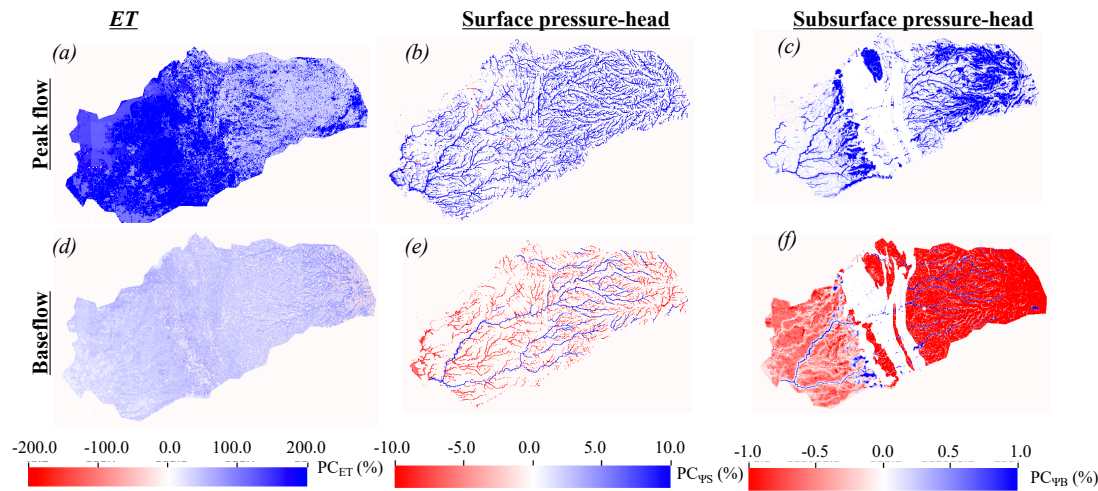


Figure 6: Comparisons between EoC median water year (WY) and the historical median WY peak flow and baseflow spatial distributions of percent changes in ET (PC_{ET}), surface water (PC_{ψ_S}) and subsurface (PC_{ψ_B}) pressure-heads. Regions in red correspond to areas with smaller fluxes or pressure-heads in the EoC compared to the historical ones, whereas regions in blue correspond to areas with larger fluxes or pressure-heads in the EoC compared to the historical WY.

1.2.2. Dry water years

Figure 7 illustrates the percent changes in ET , surface water, and subsurface pressure-heads in the EoC dry WY compared to the historical dry WY during peak flow and baseflow conditions. During peak flow conditions, the EoC dry WY has larger ET , surface, and subsurface pressure-heads than the historical dry WY (Figure 7a-c). ET is larger in this EoC dry WY not only because it is hotter, but also because there is more precipitation. Increases in surface pressure-heads are non-uniform across the domain. For example, surface water does not increase in high elevation areas (i.e., elevation > 2000m) in the EoC dry WY because the change in the precipitation phase is not significant. The main difference between the EoC and the historical dry WY is the amount

of the water flowing down gradient, which is higher in the EoC, hence the surface water in the EoC becomes higher downstream. The increase in subsurface pressure-heads in the EoC dry WY during peak flow conditions is heterogeneous with patterns similar to the changes in subsurface pressure-heads associated with the EoC median WY.

During baseflow conditions, even though ET increases in the EoC driest WY relative to the historical driest WY, surface, and subsurface pressure-heads also generally increase (Figure 7d-f). Given wetter conditions in the driest EoC WY, first-order streams are more pronounced. A few low-order streams have less surface water in the EoC when compared to the historical dry WY, similar to the results of the median WYs (see section 3.4.2). Subsurface pressure-head is generally larger in areas subject to strong connectivity with the headwaters in the EoC dry WY relative to the historical dry WY, with some regions experiencing no change from the historical conditions. This suggests that the larger amount of precipitation associated with the EoC dry WY is sufficient to supply enough water to account for high ET demands and recharge the groundwater.

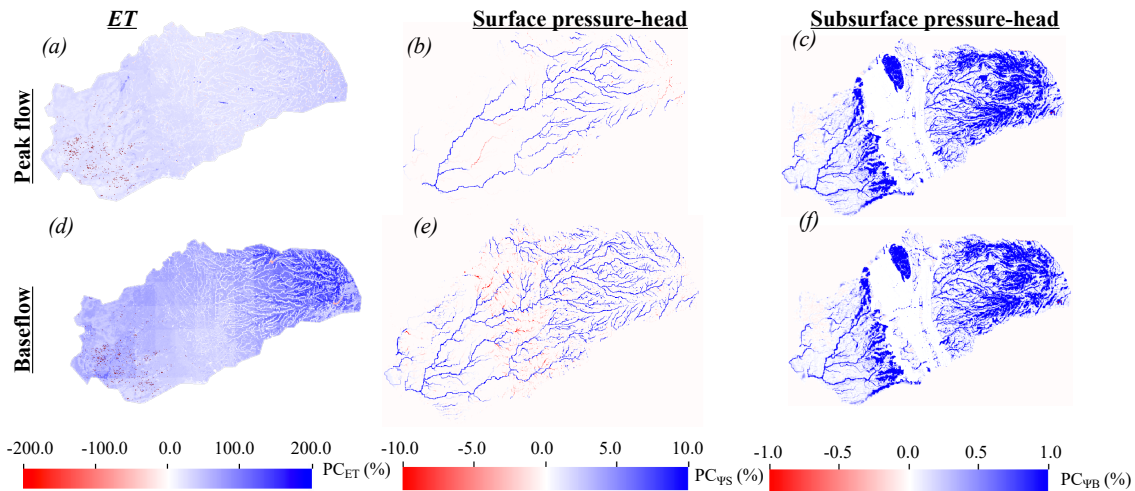


Figure 7: Comparisons between EoC dry water year (WY) and the historical dry WY peak flow and baseflow spatial distributions of percent changes in ET (PC_{ET}), surface water (PC_{ψ_S}) and subsurface (PC_{ψ_B}) pressure-heads. Regions in red correspond to areas with smaller fluxes or

pressure-heads in the EoC compared to the historical ones, whereas regions in blue correspond to areas with larger fluxes or pressure-heads in the EoC compared to the historical WY.

1.2.3. Wet water years

Figure 8 shows the percent changes in *ET*, surface water, and subsurface pressure-heads in the EoC wet WY compared to the historical wet WY during peak flow and baseflow conditions. During peak flow, the EoC wet WY is characterized by larger *ET* and subsurface pressure-heads relative to the historical wet WY and a more heterogeneous mixture of regions with both higher and lower surface water conditions throughout the catchment (Figure 8 a-c). Analogous to other WYs at EoC, the surface water pressure-head increases (decreases) are apparent in larger-order (smaller order) streams, both in the Sierra Nevada and in the Central Valley. In the wettest WY, this occurs for several reasons. First, the larger volume of precipitation, plus seasonal shifts in precipitation timing result in the filling of the higher-order streams and depletion of the lower-order streams during peak flow. Second, in the historical wet WY, a significantly greater amount of snowpack is present in the Sierra Nevada in the upper elevation of the headwaters, allowing for slower, steadier amounts of water to be released during the spring via snowmelt, and in turn, supporting low-order streams over a longer period of time. The latter effect is immediately visible in Figure 8e, where decreases in EoC surface pressure heads are visible in the headwaters, despite the watershed-total showing an increase in EoC surface water storage during baseflow (see Figure 5). Similar to the two previous EoC WYs, the subsurface pressure-head increases are shown more distinctly in the Central Valley during peak flow, under the main river channels, and in the foothills during baseflow (see previous sections on the discussion of hydroclimatic and geologic impacts).

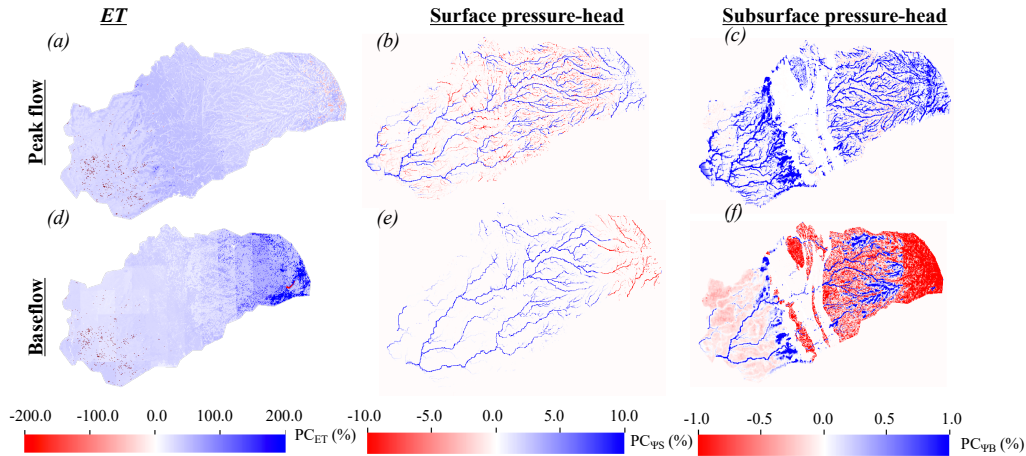


Figure 8: Comparisons between EoC wet water year (WY) and the historical wet WY peak flow and baseflow spatial distributions of percent changes in ET (PC_{ET}), surface water (PC_{ψ_S}) and subsurface (PC_{ψ_B}) pressure-heads. Regions in red correspond to areas with smaller fluxes or pressure-heads in the EoC compared to the historical ones, whereas regions in blue correspond to areas with larger fluxes or pressure-heads in the EoC compared to the historical WY.

2. Discussion

4.1 Comparison with previous studies

Some of the results presented in this study qualitatively agree with previous studies yet provide important new insights. For example, Maurer & Duffy, (2005) used 10 global climate models to project, as in this study, an increase in winter flows with an earlier peak flow timing in the WY and a decrease in summer flows. Maurer & Duffy showed mid-century projected annual precipitation and streamflow increases of 7% and 13%, respectively. Although our study focused on EoC projections, we found that compared to the historical median WY, annual surface water will increase by 19% in the EoC median WY. Compared to their findings, our work sheds light on how these changes in runoff will occur across the watershed based on its physical characteristics and highlights that while runoff will increase in the EoC, lower-order streams mainly located in the Sierra Nevada will see a decrease due to a change in precipitation phase. Mallakpour et al.,

(2018) also had a similar finding showing that future California streamflow is altered similarly to Maurer & Duffy, (2005) under both the RCP4.5 and RCP8.5 emissions scenarios, with RCP8.5 showing the highest changes during peak flow. However, contrary to our work the authors mentioned that the annual changes in streamflow will not be significant probably due to the compensation between increases in peak flow and decreases in baseflow. This was likely shaped by the differences in climate and hydrologic models used to derive these conclusions. Similar changes in streamflow were obtained by He et al., (2019) who drove the hydrologic model VIC with 10 global climate models to understand potential changes in runoff in California due to climate change. Hydrologic changes computed from the 10 global climate models were consistent and showed an increase of around 10% in annual streamflow by the late century, a percentage similar to what has been found in this study. The authors mentioned that watershed characteristics such as geology, topography, and land cover strongly impact the hydrologic response to climate change. Relationships between watershed characteristics (e.g., physiographic parameters) and its responses to climate change were further explored by Son & Tague, (2019) who highlighted that because vegetation and subsurface geology control both water availability and energy demand, they in turn influence watershed sensitivity to a changing climate, as emphasized in this study. The increases in groundwater storage shown in this study are also in agreement with Niraula et al., (2017) who used the hydrologic model VIC to show that groundwater recharge will likely increase in the northern portion of the western United States in a changing climate. Although, in this work, we show that groundwater recharge decreases in the summer in some areas due to the lack of snowmelt and higher EoC *ET*. Increases in *ET* in response to global warming has already been observed by Pascolini-Campbell et al., (2021) who showed a 10% increase in global *ET* between 2003 to 2019.

4.2 Implications for water resources management

While previous work more broadly focused on how temperature increases will alter the precipitation phase, reduce seasonal snowpack and increase winter runoff, this work brings new physical and more granular insights into how watersheds may respond to climate extremes. In particular, both wet and dry WYs in the future experience increased precipitation. As such, even in future dry WYs, water managers and stakeholders may need to prepare more for large precipitation events that may increase the possibility of flooding which requires new infrastructure management strategies. Shifts in precipitation timing, phase, and magnitude have cascading impacts on soil moisture profiles and *ET* withdrawals, which subsequently impact discharge and groundwater dynamics. Future shifts in water availability earlier in the year, as well as more dynamic transitions between peak and baseflow conditions (as quantified here), may impose stresses on water distribution, especially those systems already under scrutiny (e.g. those resources over-allocated or facing environmental degradation).

In addition, while these projections show increases in surface water and groundwater storages at watershed-scale, our results also highlight important localized spatiotemporal changes across a watershed, where the assumption of water storage increase does not necessarily hold in all geographic locations (e.g., areas that are not close to the river in the Central Valley). Our study also shows that the decreases in groundwater storage in the Central Valley aquifers are more significant than the decreases in surface water storage during baseflow conditions. This may call for new conveyance infrastructure that can move water from the relatively wetter areas to the drier areas and/or where infiltration can more readily occur. The latter suggests solutions such as Managed Aquifer Recharge (MAR) could become an increasingly important climate change adaptation. Finally, our study also highlights that lower-order streams will likely become more

ephemeral in the EoC due to flashier runoff and higher evaporative demand, such conditions will have important implications for fish spawning and ecosystem nutrient cycling.

4.3 Study limitations

In the integrated hydrologic model, the subsurface geology and land cover characterization has inherent and, in some cases, irreducible uncertainty. This study uses hydrodynamic parameters as defined by Maina et al. (2020a), which assumes that the subsurface hydrodynamics from the Sierra Nevada to the Central Valley is almost completely hydrologically separated except through overland flow. However, it is not clear whether fractures may drive more surface and subsurface flow from the headwaters to the Central Valley aquifers. In addition, we use the historical land surface cover map when simulating the EoC. It has been shown that the stomatal resistance of plants will change due to rising CO₂ with important implications for both the water and energy balance (Lemordant et al., 2018; Milly & Dunne, 2017). Future studies could assess the impact of changes in vegetation physiology and land surface cover on watershed hydrodynamics. Future studies can also estimate the impacts of different pumping and irrigation scenarios at EoC that may further impact the hydrologic system hydrodynamics in a changing climate and compare with this work. Although our VR-CESM simulations represent a cutting-edge global climate model simulation, further work may be needed to evaluate how a more refined grid resolution impacts atmospheric process representation over the Cosumnes watershed, particularly in the headwaters (Maina et al., 2020b). We further acknowledge that the 30-year simulation may not be sufficient to capture certain climate extremes (e.g., 1-in-50-year storm). Future studies, if computational resources are available, will seek to explore how the use of a longer time period might influence the identification of the most extreme dry and wet WYs from VR-CESM.

In this study, we relied on deterministic models to represent both the atmospheric (VR-CESM) and hydrologic (ParFlow-CLM) dynamics. These models are very sensitive to the initial conditions and input parameters (La Follette et al., 2021; Lehner et al., 2020; Song et al., 2015) which are uncertain given the lack of data characterizing the above and below-ground environment, including its hydrological response. Thus, while it is important to assess the sensitivity of the model outputs to these uncertain parameters, these models are computationally expensive and require many parameters. Therefore, these approaches are not feasible with the computational resources available in this study. Future work could employ reduced order models based on a subset of the physics-based model runs to explore parameter space further (e.g. Maina et al., 2022). In addition, because of the behavior of hydrological processes, the climate variability, and the uncertainties of deterministic models, model validation should ideally be performed over a long period to account for different changes and variabilities. In this study, model validation was limited to a period of 5 years due to computational constraints. Although this period encompasses the wettest and driest years on record in the region, we acknowledge that it may not be sufficient to capture the full range of hydrological variability experienced in the Cosumnes. Another limitation of using deterministic models is that the temporal variations of hydrological processes tend to follow a stochastic behavior in accordance with the so-called Hurst phenomenon (Hurst, 1951; Koutsoyiannis, 2003). As a result, these models could intensify the impacts of hydrological extremes and climate change. Finally, it has also been demonstrated that while the changes in water balance exhibit greater variability on climatic scales, the most important changes in hydrologic processes remain the overexploitation of groundwater (Ferguson and Maxwell, 2010) which has an impact on the rise in sea level (Koutsoyiannis, 2020). In addition to projecting the use of groundwater by the end of the century, future studies could compare the two approaches

(deterministic and stochastic) to better assess the limitations and the uncertainties associated with them.

5 Summary and Conclusions

Our coupled simulations project that, for the Cosumnes watershed, temperature and precipitation will both increase by the EoC across all WY types (wettest, median, and driest). In addition, precipitation is projected to occur earlier compared to historical conditions and mainly in the form of rain. For the median and wet WYs the precipitation season has earlier cessation dates, while the dry EoC WY, which is wetter than its historical counterpart, persists significantly longer into the spring. As a consequence of warmer temperatures, all WYs show a substantial decrease in *SWE*. The shift of precipitation from snowfall to rainfall, as well as the increase in the amount of precipitation and the early start of precipitation lead to an overall increase in soil moisture and more water available to meet the higher EoC *ET* demand. Importantly, this increase in *ET* is heterogeneous across the watershed and highlights one of the main advantages of using an integrated hydrologic model to assess the spatiotemporal patterns of change. Our results show that the sensitivity to the changes in *ET* at EoC depends on the subsurface geology and topographical gradients. More specifically:

- The geological and topographical complexities of the Sierra Nevada headwaters lead to highly heterogeneous changes in *ET*. Changes in *ET* are higher in permeable areas such as the plutonic rocks where water can be more easily extracted.
- *ET* changes in the Central Valley of the Cosumnes watershed are predominantly uniform with the highest sensitivities in the vicinity of the Cosumnes River due to the high availability of water.

Precipitation increases enough at EoC to provide water for both increased *ET* and increased surface water storage. Surface water storages also increase earlier in the WY and have higher peak amounts. These earlier and larger increases are a direct consequence of an earlier start in precipitation at EoC, a marked change in the precipitation phase, and an overall larger amount of precipitation when compared with the historical WYs. However, our results also highlight that during baseflow conditions surface water decreases, especially in lower-order streams, showing that these areas are highly sensitive to changes in precipitation phase. Our simulations also show that the seasonal variability of the EoC watershed behavior is also more dynamic. In general, decreases in seasonal water storages occurring between peak flow and baseflow conditions are more than 10% higher in the EoC compared to the historical conditions.

EoC groundwater storages are also projected to increase earlier in the WY with peaks greater than those found historically. Yet these storages decrease significantly during baseflow conditions due to the higher *ET* at EoC and the absence of recharge from snowmelt. Contrary to the changes in surface water storages, groundwater storages show a larger decrease due to their dependence on the surface water from the Sierra Nevada. Our results also show that changes in subsurface pressure-heads are not uniform and are bi-directional throughout the Cosumnes watershed. Because the connectivity between the Central Valley aquifers and the Sierra Nevada headwaters (i.e., subsurface and surface flows from the headwater to the Central Valley aquifers) plays an important role in the hydrodynamics of this watershed, only areas with a strong connection with the headwaters, such as the foothills and the river channels, see an increase in subsurface pressure-heads at EoC. However, the subsurface pressure-heads decrease elsewhere in the Central Valley aquifers especially in baseflow conditions due to the high *ET* and the lack of snowmelt. In

the river channels, this is due to the exchange between the subsurface and the surface whereas the foothills characterized by the consolidated sediments serve as “spillover.”

Our results provide novel understandings about possible changes in the integrated hydrologic response to changes in EoC climate extremes. An important caveat is that our simulation was a single set of climate realizations and may not properly bound internal climate variability uncertainty like an ensemble of climate simulations could. However, beyond the widely agreed-upon changes of decreased snowpack and shifts in runoff timing in the literature, we show that in this simulation: 1) EoC precipitation increases even in the driest years; 2) despite an increased temperature, and hence *ET*, both groundwater and surface water storage increase relative to historical conditions because of increased precipitation; and 3) there is a distinct spatial pattern, particularly in surface water storage, in which smaller-order streams see reduced flow while the larger order streams see an increased flow. These changes will have strong implications on natural resource management.

Data availability

Data supporting the findings of this study can be found here:

<https://portal.nersc.gov/archive/home/a/arhoades/Shared/www/Hyperion/>

Author contribution

The authors contribute equally to this work.

Competing interests

The authors declare that they have no conflict of interest.

Acknowledgements

Fadji Zaoua Maina and Erica Siirila-Woodburn were supported by LDRD funding from Berkeley Lab, provided by the Director, Office of Science, of the U.S. Department of Energy under Contract No. DE-AC02-05CH11231.

Author Alan M. Rhoades was funded by the Department of Energy, Office of Science Office of Biological and Environmental Research program under Award Number DE-SC0016605 "A framework for improving analysis and modeling of Earth system and intersectoral dynamics at regional scales" and Award Number DE-AC02-05CH11231 "The Calibrated and Systematic Characterization, Attribution, and Detection of Extremes - Science Focus Area".

This research used computing resources from the National Energy Research Scientific Computing Center, a DOE Office of Science User Facility supported by the <http://dx.doi.org/10.13039/100006132> of the U.S. Department of Energy under Contract No. DE-AC02-05CH11231.

References

- Abbott, M. B., J. C. Bathurst, J. A. Cunge, P. E. Oconnell, and J. Rasmussen (1986), An introduction to the european hydrological system: Sys- teme hydrologique Europeen, She .2. Structure of a physically-based, distributed modeling system, *J. Hydrol.*, 87(1–2), 61–77.
- Allan, R.P., Barlow, M., Byrne, M.P., Cherchi, A., Douville, H., Fowler, H.J., Gan, T.Y., Pendergrass, A.G., Rosenfeld, D., Swann, A.L.S., Wilcox, L.J. and Zolina, O. (2020), Advances in understanding large-scale responses of the water cycle to climate change. *Ann. N.Y. Acad. Sci.*, 1472: 49-75. <https://doi.org/10.1111/nyas.14337>
- Allen R. G., Masahiro T., Ricardo T. (2007) Satellite-based energy balance for mapping evapotranspiration with internalized calibration (METRIC)—model J. *Irrig. Drain. Eng.*, 133, pp. 380-394, 10.1061/(ASCE)0733-9437(2007) 133:4(380).
- Alo, C. A., & Wang, G. (2008). Hydrological impact of the potential future vegetation response to climate changes projected by 8 GCMs. *Journal of Geophysical Research: Biogeosciences*, 113(G3). <https://doi.org/10.1029/2007JG000598>
- Bair E.H., Rittger K., Davis R.E., Painter T.H., Dozier J. (2016) Validating reconstruction of snow water equivalent in California’s Sierra Nevada using measurements from the NASA Airborne Snow Observatory *Water Resour. Res.*, 52 , pp. 8437-8460, 10.1002/2016WR018704
- Bales, R. C., Molotch, N. P., Painter, T. H., Dettinger, M. D., Rice, R., & Dozier, J. (2006). Mountain hydrology of the western United States. *Water Resources Research*, 42(8). <https://doi.org/10.1029/2005WR004387>

- Barnett, T. P., Adam, J. C., & Lettenmaier, D. P. (2005). Potential impacts of a warming climate on water availability in snow-dominated regions. *Nature*, 438(7066), 303–309. <https://doi.org/10.1038/nature04141>
- Berghuijs, W. R., Woods, R. A., & Hrachowitz, M. (2014). A precipitation shift from snow towards rain leads to a decrease in streamflow. *Nature Climate Change*, 4(7), 583–586. <https://doi.org/10.1038/nclimate2246>
- Bixio, A. C., G. Gambolati, C. Paniconi, M. Putti, V. M. Shestopalov, V. N. Bublias, A. S. Bohuslavsky, N. B. Kasteltseva, and Y. F. Rudenko (2002), Modeling groundwater-surface water interactions including effects of morphogenetic depressions in the Chernobyl exclusion zone, *Environ. Geol.*, 42(2-3) 162-177.
- Cayan, D. R., Maurer, E. P., Dettinger, M. D., Tyree, M., & Hayhoe, K. (2008). Climate change scenarios for the California region. *Climatic Change*, 87(1), 21–42. <https://doi.org/10.1007/s10584-007-9377-6>
- Christensen, L., Tague, C. L., & Baron, J. S. (2008). Spatial patterns of simulated transpiration response to climate variability in a snow dominated mountain ecosystem. *Hydrological Processes*, 22(18), 3576–3588. <https://doi.org/10.1002/hyp.6961>
- Collins, W. D., Bitz, C. M., Blackmon, M. L., Bonan, G. B., Bretherton, C. S., Carton, J. A., et al. (2006). The Community Climate System Model Version 3 (CCSM3). *Journal of Climate*, 19(11), 2122–2143. <https://doi.org/10.1175/JCLI3761.1>
- Condon, L. E., Maxwell, R. M., & Gangopadhyay, S. (2013). The impact of subsurface conceptualization on land energy fluxes. *Advances in Water Resources*, 60, 188–203. <https://doi.org/10.1016/j.advwatres.2013.08.001>

- Condon, L.E., Atchley, A.L., Maxwell, R.M., (2020). Evapotranspiration depletes groundwater under warming over the contiguous United States. *Nature Communications* 11, 873. <https://doi.org/10.1038/s41467-020-14688-0>
- Cook, E. R., Woodhouse, C. A., Eakin, C. M., Meko, D. M., & Stahle, D. W. (2004). Long-Term Aridity Changes in the Western United States. *Science*, 306(5698), 1015–1018. <https://doi.org/10.1126/science.1102586>
- Coon, E. T., J. D. Moulton, and S. L. Painter (2016), Managing complexity in simulations of land surface and near-surface processes, *Environ. Modell Software*, 78, 134-149.
- Cosgrove, B. A., Lohmann, D., Mitchell, K. E., Houser, P. R., Wood, E. F., Schaake, J. C., et al. (2003). Real-time and retrospective forcing in the North American Land Data Assimilation System (NLDAS) project. *Journal of Geophysical Research: Atmospheres*, 108(D22). <https://doi.org/10.1029/2002JD003118>
- Cristea, N. C., Lundquist, J. D., Loheide, S. P., Lowry, C. S., & Moore, C. E. (2014). Modelling how vegetation cover affects climate change impacts on streamflow timing and magnitude in the snowmelt-dominated upper Tuolumne Basin, Sierra Nevada. *Hydrological Processes*, 28(12), 3896–3918. <https://doi.org/10.1002/hyp.9909>
- Daly, C., Halbleib, M., Smith, J. I., Gibson, W. P., Doggett, M. K., Taylor, G. H., et al. (2008). Physiographically sensitive mapping of climatological temperature and precipitation across the conterminous United States. *International Journal of Climatology*, 28(15), 2031–2064. <https://doi.org/10.1002/joc.1688>.
- Dettinger, M. (2011). Climate Change, Atmospheric Rivers, and Floods in California – A Multimodel Analysis of Storm Frequency and Magnitude Changes¹. *JAWRA Journal of*

- the American Water Resources Association*, 47(3), 514–523.
<https://doi.org/10.1111/j.1752-1688.2011.00546.x>
- Dettinger, M., & Anderson, M. L. (2015). Storage in California's reservoirs and snowpack in this time of drought. *San Francisco Estuary and Watershed Science*, 13(2).
<https://doi.org/10.15447/sfews.2015v13iss2art1>
- Dettinger, M., Redmond, K., & Cayan, D. (2004). Winter Orographic Precipitation Ratios in the Sierra Nevada—Large-Scale Atmospheric Circulations and Hydrologic Consequences. *Journal of Hydrometeorology*, 5(6), 1102–1116. <https://doi.org/10.1175/JHM-390.1>
- Dettinger, M. D. (2013). Atmospheric Rivers as Drought Busters on the U.S. West Coast. *Journal of Hydrometeorology*, 14(6), 1721–1732. <https://doi.org/10.1175/JHM-D-13-02.1>
- Di Liberto, T. (2017, October). Very wet 2017 WY ends in California. *NOAA Climate.Gov*. Retrieved from <https://www.climate.gov/news-features/featured-images/very-wet-2017-water-year-ends-california>
- Dierauer, J. R., Whitfield, P. H., & Allen, D. M. (2018). Climate Controls on Runoff and Low Flows in Mountain Catchments of Western North America. *Water Resources Research*, 54(10), 7495–7510. <https://doi.org/10.1029/2018WR023087>
- Faunt, C.C., Belitz, K., Hanson, R.T., 2010. Development of a three-dimensional model of sedimentary texture in valley-fill deposits of Central Valley, California, USA. *Hydrogeology Journal* 18, 625–649. <https://doi.org/10.1007/s10040-009-0539-7>
- Faunt, C.C., Geological Survey (U.S.) (Eds.), 2009. Groundwater availability of the Central Valley Aquifer, California, U.S. Geological Survey professional paper. U.S. Geological Survey, Reston, Va.

- Ferguson, I. M. and Maxwell, R. M. (2010) Role of groundwater in watershed response and land surface feedbacks under climate change, *Water Resour. Res.*, 46, 1–15, <https://doi.org/10.1029/2009WR008616>.
- Ficklin, D. L., Luo, Y., & Zhang, M. (2013). Climate change sensitivity assessment of streamflow and agricultural pollutant transport in California’s Central Valley using Latin hypercube sampling. *Hydrological Processes*, 27(18), 2666–2675. <https://doi.org/10.1002/hyp.9386>
- Foster, L. M., Williams, K. H., & Maxwell, R. M. (2020). Resolution matters when modeling climate change in headwaters of the Colorado River. *Environmental Research Letters*. <https://doi.org/10.1088/1748-9326/aba77f>
- Gates WL (1992) AMIP: the atmospheric model intercomparison project. *Bull Am Meteorol Soc* 73(12):1962–1970. doi:10.1175/1520-0477(1992)073<1962:ATAMIP>2.0.CO;2
- Geologic Map of California, 2015. Geologic Map of California [WWW Document]. Geologic Map of California. URL <https://maps.conservation.ca.gov/cgs/gmc/> (accessed 10.17.18).
- Gent, P. R., Danabasoglu, G., Donner, L. J., Holland, M. M., Hunke, E. C., Jayne, S. R., et al. (2011). The Community Climate System Model Version 4. *Journal of Climate*, 24(19), 4973–4991. <https://doi.org/10.1175/2011JCLI4083.1>
- Gershunov, A., Shulgina, T., Clemesha, R.E.S. et al. (2019). Precipitation regime change in Western North America: The role of Atmospheric Rivers. *Sci Rep* 9, 9944. <https://doi.org/10.1038/s41598-019-46169-w>
- Gettelman, A., and Morrison, H. (2015). Advanced Two-Moment Bulk Microphysics for Global Models. Part I: Off-Line Tests and Comparison with Other Schemes. *Journal of Climate* 28, 3, 1268-1287. <https://doi.org/10.1175/JCLI-D-14-00102.1>

- Gilbert, J.M., Maxwell, R.M., 2017. Examining regional groundwater - surface water dynamics using an integrated hydrologic model of the San Joaquin River basin. *Hydrology and Earth System Sciences* 21, 923–947. <https://doi.org/10.5194/hess-21-923-2017>
- Gleick, P. H. (1987). The development and testing of a water balance model for climate impact assessment: Modeling the Sacramento Basin. *Water Resources Research*, 23(6), 1049–1061. <https://doi.org/10.1029/WR023i006p01049>
- Godsey, S. E., Kirchner, J. W., & Tague, C. L. (2014). Effects of changes in winter snowpacks on summer low flows: case studies in the Sierra Nevada, California, USA. *Hydrological Processes*, 28(19), 5048–5064. <https://doi.org/10.1002/hyp.9943>
- Griffin, D., & Anchukaitis, K. J. (2014). How unusual is the 2012–2014 California drought? *Geophysical Research Letters*, 41(24), 9017–9023. <https://doi.org/10.1002/2014GL062433>
- Haarsma, R. J., Roberts, M. J., Vidale, P. L., Senior, C. A., Bellucci, A., Bao, Q., Chang, P., Corti, S., Fučkar, N. S., Guemas, V., von Hardenberg, J., Hazeleger, W., Kodama, C., Koenigk, T., Leung, L. R., Lu, J., Luo, J.-J., Mao, J., Mizielinski, M. S., Mizuta, R., Nobre, P., Satoh, M., Scoccimarro, E., Semmler, T., Small, J., and von Storch, J.-S. (2016). High Resolution Model Intercomparison Project (HighResMIP v1.0) for CMIP6, *Geosci. Model Dev.*, 9, 4185–4208, <https://doi.org/10.5194/gmd-9-4185-2016>.
- Harbaugh AW (2005) MODFLOW-2005, The U.S. Geological Survey modular ground-water model: the ground-water flow process. US Geol Surv Tech Methods 6-A16. <http://pubs.usgs.gov/tm/2005/tm6A16/>.

- Harpold, A. A., & Molotch, N. P. (2015). Sensitivity of soil water availability to changing snowmelt timing in the western U.S. *Geophysical Research Letters*, *42*(19), 8011–8020. <https://doi.org/10.1002/2015GL065855>
- Hayhoe, K., Cayan, D., Field, C. B., Frumhoff, P. C., Maurer, E. P., Miller, N. L., et al. (2004). Emissions pathways, climate change, and impacts on California. *Proceedings of the National Academy of Sciences*, *101*(34), 12422–12427. <https://doi.org/10.1073/pnas.0404500101>
- He, M., Anderson, M., Schwarz, A., Das, T., Lynn, E., Anderson, J., et al. (2019). Potential Changes in Runoff of California’s Major Water Supply Watersheds in the 21st Century. *Water*, *11*(8), 1651. <https://doi.org/10.3390/w11081651>
- Herrington, A. R., P. H. Lauritzen, M. A. Taylor, S. Goldhaber, B. E. Eaton, J. T. Bacmeister, K. A. Reed, and P. A. Ullrich (2019). Physics–Dynamics Coupling with Element-Based High-Order Galerkin Methods: Quasi-Equal-Area Physics Grid. *Mon. Wea. Rev.*, *147*, 69–84, <https://doi.org/10.1175/MWR-D-18-0136.1>.
- Homer, C., Dewitz, J., Yang, L., Jin, S., Danielson, P., Xian, G., et al. (2015). Completion of the 2011 National Land Cover Database for the conterminous United States—representing a decade of land cover change information. *Photogrammetric Engineering & Remote Sensing*, *81*(5), 345–354.
- Huang, X., Rhoades, A. M., Ullrich, P. A., & Zarzycki, C. M. (2016). An evaluation of the variable-resolution CESM for modeling California’s climate. *Journal of Advances in Modeling Earth Systems*, *8*(1), 345–369. <https://doi.org/10.1002/2015MS000559>
- Huang, X., Stevenson, S., & Hall, A. D. (2020). Future warming and intensification of precipitation extremes: A “double whammy” leading to increasing flood risk in California.

Geophysical Research Letters, 47, e2020GL088679.
<https://doi.org/10.1029/2020GL088679>

Hurrell, J. W., Holland, M. M., Gent, P. R., Ghan, S., Kay, J. E., Kushner, P. J., et al. (2013). The Community Earth System Model: A Framework for Collaborative Research. *Bulletin of the American Meteorological Society*, 94(9), 1339–1360. <https://doi.org/10.1175/BAMS-D-12-00121.1>

Hurst. (1951) Long-Term Storage Capacity of Reservoirs, *Trans. Am. Soc. Civ. Eng.*, 116, 770–799.

Jones, P. W., (1999). First- and Second-Order Conservative Remapping Schemes for Grids in Spherical Coordinates. *Mon. Wea. Rev.*, 127, 2204–2210, [https://doi.org/10.1175/1520-0493\(1999\)127<2204:FASOCR>2.0.CO;2](https://doi.org/10.1175/1520-0493(1999)127<2204:FASOCR>2.0.CO;2).

IGBP, 2018. Global plant database published - IGBP [WWW Document]. URL <http://www.igbp.net/news/news/news/globalplantdatabasepublished.5.1b8ae20512db692f2a6800014762.html> (accessed 10.17.18).

Jennings, C. W., Strand, R. G., & Rogers, T. H. (1977). *Geologic map of California*. Sacramento, Calif.: Division of Mines and Geology.

Kampenhout, L. van, Rhoades, A. M., Herrington, A. R., Zarzycki, C. M., Lenaerts, J. T. M., Sacks, W. J., & Broeke, M. R. van den. (2019). Regional grid refinement in an Earth system model: impacts on the simulated Greenland surface mass balance. *The Cryosphere*, 13(6), 1547–1564. <https://doi.org/10.5194/tc-13-1547-2019>

Kollet, S. J., & Maxwell, R. M. (2006). Integrated surface–groundwater flow modeling: A free-surface overland flow boundary condition in a parallel groundwater flow model. *Advances in Water Resources*, 29(7), 945–958. <https://doi.org/10.1016/j.advwatres.2005.08.006>

- Koutsoyiannis, D (2003) Climate change, the Hurst phenomenon, and hydrological statistics, *Hydrological Sciences Journal*, 48:1, 3-24, DOI: 10.1623/hysj.48.1.3.43481
- Koutsoyiannis, D., (2020) Revisiting the global hydrological cycle: is it intensifying?, *Hydrology and Earth System Sciences*, 24, 3899–3932, doi:10.5194/hess-24-3899-2020.
- La Follette, P. T., Teuling, A. J., Addor, N., Clark, M., Jansen, K., & Melsen, L. A. (2021). Numerical daemons of hydrological models are summoned by extreme precipitation. *Hydrology and Earth System Sciences*, 25(10), 5425–5446. <https://doi.org/10.5194/hess-25-5425-2021>
- Lehner, F., Deser, C., Maher, N., Marotzke, J., Fischer, E. M., Brunner, L., et al. (2020). Partitioning climate projection uncertainty with multiple large ensembles and CMIP5/6. *Earth System Dynamics*, 11(2), 491–508. <https://doi.org/10.5194/esd-11-491-2020>
- Lemordant, L., Gentine, P., Swann, A. S., Cook, B. I., & Scheff, J. (2018). Critical impact of vegetation physiology on the continental hydrologic cycle in response to increasing CO₂. *Proceedings of the National Academy of Sciences*, 115(16), 4093–4098. <https://doi.org/10.1073/pnas.1720712115>
- Liang, X., D. P. Lettenmaier, E. F. Wood, and S. J. Burges (1994), A simple hydrologically based model of land surface water and energy fluxes for general circulation models, *J. Geophys. Res.*, 99(D7), 14415–14428, doi:10.1029/94JD00483.
- Lundquist, J. D., Hughes, M., Henn, B., Gutmann, E. D., Livneh, B., Dozier, J., & Neiman, P. (2015). High-Elevation Precipitation Patterns: Using Snow Measurements to Assess Daily Gridded Datasets across the Sierra Nevada, California, *Journal of Hydrometeorology*, 16(4), 1773-1792. doi: https://journals.ametsoc.org/view/journals/hydr/16/4/jhm-d-15-0019_1.xml

- Maina, Fadji Z., Siirila-Woodburn, E. R., Newcomer, M., Xu, Z., & Steefel, C. (2020a). Determining the impact of a severe dry to wet transition on watershed hydrodynamics in California, USA with an integrated hydrologic model. *Journal of Hydrology*, 580, 124358. <https://doi.org/10.1016/j.jhydrol.2019.124358>
- Maina, F. Z., Siirila-Woodburn, E. R., & Vahmani, P. (2020b). Sensitivity of meteorological-forcing resolution on hydrologic variables. *Hydrology and Earth System Sciences*, 24(7), 3451–3474. <https://doi.org/10.5194/hess-24-3451-2020>
- Maina, Fadji Zaouna, & Siirila-Woodburn, E. R. (2020c). Watersheds dynamics following wildfires: Nonlinear feedbacks and implications on hydrologic responses. *Hydrological Processes*, 34(1), 33–50. <https://doi.org/10.1002/hyp.13568>
- Maina, Fadji Z., Siirila-Woodburn, E. R., & Denny-Frank, P. J. (2022) Assessing the impacts of hydrodynamic parameter uncertainties on simulated evapotranspiration in a mountainous watershed. *Journal of Hydrology* 608. <https://doi.org/10.1016/j.jhydrol.2022.127620>.
- Mallakpour, I., Sadegh, M., AghaKouchak, A., 2018. A new normal for streamflow in California in a warming climate: Wetter wet seasons and drier dry seasons. *Journal of Hydrology* 567, 203–211. <https://doi.org/10.1016/j.jhydrol.2018.10.023>
- Maurer, E. P. (2007). Uncertainty in hydrologic impacts of climate change in the Sierra Nevada, California, under two emissions scenarios. *Climatic Change*, 82(3), 309–325. <https://doi.org/10.1007/s10584-006-9180-9>
- Maurer, E. P., & Duffy, P. B. (2005). Uncertainty in projections of streamflow changes due to climate change in California. *Geophysical Research Letters*, 32(3). <https://doi.org/10.1029/2004GL021462>

- Maxwell, R. M. (2013). A terrain-following grid transform and preconditioner for parallel, large-scale, integrated hydrologic modeling. *Advances in Water Resources*, 53, 109–117. <https://doi.org/10.1016/j.advwatres.2012.10.001>
- Maxwell, R. M., & Condon, L. E. (2016). Connections between groundwater flow and transpiration partitioning. *Science*, 353(6297), 377–380. <https://doi.org/10.1126/science.aaf7891>
- Maxwell, R. M., & Miller, N. L. (2005). Development of a Coupled Land Surface and Groundwater Model. *Journal of Hydrometeorology*, 6(3), 233–247. <https://doi.org/10.1175/JHM422.1>
- Mayer, T. D., & Naman, S. W. (2011). Streamflow Response to Climate as Influenced by Geology and Elevation. *JAWRA Journal of the American Water Resources Association*, 47(4), 724–738. <https://doi.org/10.1111/j.1752-1688.2011.00537.x>
- Boryan, C., Yang, Z., Mueller, R., Craig, M., 2011. Monitoring US agriculture: the US Department of Agriculture, National Agricultural Statistics Service, Cropland Data Layer Program. *Geocarto International* 26, 341–358. <https://doi.org/10.1080/10106049.2011.562309>
- Mallakpour, I., Sadegh, M., AghaKouchak, A., 2018. A new normal for streamflow in California in a warming climate: Wetter wet seasons and drier dry seasons. *Journal of Hydrology* 567, 203–211. <https://doi.org/10.1016/j.jhydrol.2018.10.023>
- Maxwell, R.M., 2013. A terrain-following grid transform and preconditioner for parallel, large-scale, integrated hydrologic modeling. *Advances in Water Resources* 53, 109–117. <https://doi.org/10.1016/j.advwatres.2012.10.001>
- McEvoy, D.J., Pierce, D.W., Kalansky, J.F., Cayan, D.R., Abatzoglou, J.T., 2020. Projected Changes in Reference Evapotranspiration in California and Nevada: Implications for

- Drought and Wildland Fire Danger. *Earth's Future* 8, e2020EF001736.
<https://doi.org/10.1029/2020EF001736>
- Milly, P. C. D., & Dunne, K. A. (2017). A Hydrologic Drying Bias in Water-Resource Impact Analyses of Anthropogenic Climate Change. *JAWRA Journal of the American Water Resources Association*, 53(4), 822–838. <https://doi.org/10.1111/1752-1688.12538>
- Milly, P. C. D., Dunne, K. A., & Vecchia, A. V. (2005). Global pattern of trends in streamflow and water availability in a changing climate. *Nature*, 438(7066), 347–350. <https://doi.org/10.1038/nature04312>
- Mote, P. W., Hamlet, A. F., Clark, M. P., & Lettenmaier, D. P. (2005). Declining mountain snowpack in western north america*. *Bulletin of the American Meteorological Society*, 86(1), 39–50. <https://doi.org/10.1175/BAMS-86-1-39>
- Musselman, K. N., Clark, M. P., Liu, C., Ikeda, K., & Rasmussen, R. (2017). Slower snowmelt in a warmer world. *Nature Climate Change*, 7(3), 214–219. <https://doi.org/10.1038/nclimate3225>
- Musselman, K. N., Molotch, N. P., & Margulis, S. A. (2017). Snowmelt response to simulated warming across a large elevation gradient, southern Sierra Nevada, California. *The Cryosphere*, 11(6), 2847–2866. <https://doi.org/10.5194/tc-11-2847-2017>
- National Operational Hydrologic Remote Sensing Center. (2004). Snow Data Assimilation System (SNODAS) Data Products at NSIDC. <https://doi.org/10.7265/N5TB14TC>.
- Neelin, J. D., Langenbrunner, B., Meyerson, J. E., Hall, A., & Berg, N. (2013). California Winter Precipitation Change under Global Warming in the Coupled Model Intercomparison Project Phase 5 Ensemble. *Journal of Climate*, 26(17), 6238–6256. <https://doi.org/10.1175/JCLI-D-12-00514.1>

- Neitsch, S. L., Arnold, J. G., Kiniry, J. R., & Williams, J. R. (2001). Soil and Water Assessment tool (SWAT) user's manual version 2000. Grassland Soil and Water Research Laboratory. Temple, TX: ARS.
- Niraula, R., Meixner, T., Dominguez, F., Bhattarai, N., Rodell, M., Ajami, H., et al. (2017). How Might Recharge Change Under Projected Climate Change in the Western U.S.? *Geophysical Research Letters*, 44(20), 10,407-10,418. <https://doi.org/10.1002/2017GL075421>
- Niu, G.-Y., et al. (2011), The community Noah land surface model with multiparameterization options (Noah-MP): 1. Model description and evaluation with local-scale measurements. *J. Geophys. Res.*, 116, D12109, doi: 10.1029/2010JD015139.
- SMAP. (2015). Soil Moisture Active Passive. Retrieved October 18, 2018, from SMAP website: <https://smap.jpl.nasa.gov/>
- Siirila-Woodburn, E. R., Rhoades, A. M., Hatchett, B. J., Huning, L. S., Szinai, J., Tague, C., Nico, P. S., Feldman, D. R., Jones, A. D., Collins, W. D., and Kaatz, L.: A low-to-no snow future and its impacts on water resources in the western United States, *Nature Reviews Earth and Environment*, <https://doi.org/10.1038/s43017-021-00219-y>, 2021.
- Pascolini-Campbell, M., Reager, J. T., Chandanpurkar, H. A., & Rodell, M. (2021). A 10 per cent increase in global land evapotranspiration from 2003 to 2019. *Nature*, 593(7860), 543–547. <https://doi.org/10.1038/s41586-021-03503-5>
- Payne, A. E., Demory, M.-E., Leung, L. R., Ramos, A. M., Shields, C. A., Rutz, J. J., et al. (2020). Responses and impacts of atmospheric rivers to climate change. *Nature Reviews Earth & Environment*, 1(3), 143–157. <https://doi.org/10.1038/s43017-020-0030-5>

- Persad, G. G., Swain, D. L., Kouba, C., & Ortiz-Partida, J. P. (2020). Inter-model agreement on projected shifts in California hydroclimate characteristics critical to water management. *Climatic Change*, 162(3), 1493–1513. <https://doi.org/10.1007/s10584-020-02882-4>
- Ralph, F. M., & Dettinger, M. D. (2011). Storms, floods, and the science of atmospheric rivers. *Eos, Transactions American Geophysical Union*, 92(32), 265–266. <https://doi.org/10.1029/2011EO320001>
- Ralph, F. Martin, Neiman, P. J., Wick, G. A., Gutman, S. I., Dettinger, M. D., Cayan, D. R., & White, A. B. (2006). Flooding on California's Russian River: Role of atmospheric rivers. *Geophysical Research Letters*, 33(13). <https://doi.org/10.1029/2006GL026689>
- Rasmussen, R., Liu, C., Ikeda, K., Gochis, D., Yates, D., Chen, F., et al. (2011). High-Resolution Coupled Climate Runoff Simulations of Seasonal Snowfall over Colorado: A Process Study of Current and Warmer Climate. *Journal of Climate*, 24(12), 3015–3048. <https://doi.org/10.1175/2010JCLI3985.1>
- Rhoades, A. M., Huang, X., Ullrich, P. A., & Zarzycki, C. M. (2016). Characterizing Sierra Nevada Snowpack Using Variable-Resolution CESM. *Journal of Applied Meteorology and Climatology*, 55(1), 173–196. <https://doi.org/10.1175/JAMC-D-15-0156.1>
- Rhoades, A. M., Ullrich, P. A., & Zarzycki, C. M. (2018a). Projecting 21st century snowpack trends in western USA mountains using variable-resolution CESM. *Climate Dynamics*, 50(1), 261–288. <https://doi.org/10.1007/s00382-017-3606-0>
- Rhoades, A. M., Jones, A. D., & Ullrich, P. A. (2018b). The changing character of the California Sierra Nevada as a natural reservoir. *Geophysical Research Letters*, 45, 13,008– 13,019. <https://doi.org/10.1029/2018GL080308>

- Rhoades, A. M., Ullrich, P. A., Zarzycki, C. M., Johansen, H., Margulis, S. A., Morrison, H., et al. (2018c). Sensitivity of Mountain Hydroclimate Simulations in Variable-Resolution CESM to Microphysics and Horizontal Resolution. *Journal of Advances in Modeling Earth Systems*, 10(6), 1357–1380. <https://doi.org/10.1029/2018MS001326>
- Rhoades, A. M., Jones, A. D., O'Brien, T. A., O'Brien, J. P., Ullrich, P. A., & Zarzycki, C. M. (2020a). Influences of North Pacific Ocean domain extent on the western U.S. winter hydroclimatology in variable-resolution CESM. *Journal of Geophysical Research: Atmospheres*, 125, e2019JD031977. <https://doi.org/10.1029/2019JD031977>
- Rhoades, A. M., Jones, A. D., Srivastava, A., Huang, H., O'Brien, T. A., Patricola, C. M., et al. (2020b). The shifting scales of western U.S. landfalling atmospheric rivers under climate change. *Geophysical Research Letters*, 47, e2020GL089096. <https://doi.org/10.1029/2020GL089096>
- Rhoades, A. M., Risser, M. D., Stone, D. A., Wehner, M. F., & Jones, A. D. (2021). Implications of warming on western United States landfalling atmospheric rivers and their flood damages. *Weather and Climate Extremes*, 32, 100326, <https://doi.org/10.1016/j.wace.2021.100326>
- Richards, L. A. (1931). Capillary conduction of liquids through porous medium. *Journal of Applied Physics*, 1(5), 318–333. <https://doi.org/10.1063/1.1745010>
- Safeeq, M., Grant, G. E., Lewis, S. L., Kramer, M. G., & Staab, B. (2014). A hydrogeologic framework for characterizing summer streamflow sensitivity to climate warming in the Pacific Northwest, USA. *Hydrology and Earth System Sciences*, (18), 1–8. <https://doi.org/10.5194/hess-18-3693-2014>

- Safeeq, M., Grant, G.E., Lewis, S.L. and Tague, C.L. (2013), Coupling snowpack and groundwater dynamics to interpret historical streamflow trends in the western United States. *Hydrological Processes*, 27: 655-668. <https://doi.org/10.1002/hyp.9628>
- Safeeq, Mohammad, Grant, G. E., Lewis, S. L., & Staab, B. (2015). Predicting landscape sensitivity to present and future floods in the Pacific Northwest, USA. *Hydrological Processes*, 29(26), 5337–5353. <https://doi.org/10.1002/hyp.10553>
- SCRIPPS Institution of Oceanography. (2017, April). Northern California Just Surpassed the Wettest Year on Record | Scripps Institution of Oceanography, UC San Diego. Retrieved from <https://scripps.ucsd.edu/news/northern-california-just-surpassed-wettest-year-record>
- Shukla, S., Safeeq, M., AghaKouchak, A., Guan, K., & Funk, C. (2015). Temperature impacts on the WY 2014 drought in California. *Geophysical Research Letters*, 4384–4393. [https://doi.org/10.1002/2015GL063666@10.1002/\(ISSN\)1944-8007.CALDROUGHT1](https://doi.org/10.1002/2015GL063666@10.1002/(ISSN)1944-8007.CALDROUGHT1)
- Son, K., & Tague, C. (2019). Hydrologic responses to climate warming for a snow-dominated watershed and a transient snow watershed in the California Sierra. *Ecohydrology*, 12(1), e2053. <https://doi.org/10.1002/eco.2053>
- Song, X., Zhang, J., Zhan, C., Xuan, Y., Ye, M., Xu C., (2015) Global sensitivity analysis in hydrological modeling: Review of concepts, methods, theoretical framework, and applications. *Journal of Hydrology*, 523 pp. 739-757, 10.1016/j.jhydrol.2015.02.013
- Strachan, S., and Daly, C. (2017), Testing the daily PRISM air temperature model on semiarid mountain slopes, *J. Geophys. Res. Atmos.*, 122, 5697– 5715, doi:10.1002/2016JD025920.
- Swain, D. L., Langenbrunner, B., Neelin, J. D., & Hall, A. (2018). Increasing precipitation volatility in twenty-first-century California. *Nature Climate Change*, 8(5), 427–433. <https://doi.org/10.1038/s41558-018-0140-y>

- Tague, C., & Peng, H. (2013). The sensitivity of forest water use to the timing of precipitation and snowmelt recharge in the California Sierra: Implications for a warming climate. *Journal of Geophysical Research: Biogeosciences*, 118(2), 875–887. <https://doi.org/10.1002/jgrg.20073>
- Tang, G., Li, S., Yang, M., Xu, Z., Liu, Y., & Gu, H. (2019). Streamflow response to snow regime shift associated with climate variability in four mountain watersheds in the US Great Basin. *Journal of Hydrology*, 573, 255–266. <https://doi.org/10.1016/j.jhydrol.2019.03.021>
- The NCAR Command Language (Version 6.6.2) (2021). Boulder, Colorado: UCAR/NCAR/CISL/TDD, 851 <http://dx.doi.org/10.5065/D6WD3XH5>.
- Trefry, M.G.; Muffels, C. (2007). "FEFLOW: a finite-element ground water flow and transport modeling tool". *Ground Water*. 45 (5): 525–528. doi:10.1111/j.1745-6584.2007.00358.x
- Vicuna, S., & Dracup, J. A. (2007). The evolution of climate change impact studies on hydrology and water resources in California. *Climatic Change*, 82(3), 327–350. <https://doi.org/10.1007/s10584-006-9207-2>
- Vicuna, Sebastian, Maurer, E. P., Joyce, B., Dracup, J. A., & Purkey, D. (2007). The Sensitivity of California Water Resources to Climate Change Scenarios1. *JAWRA Journal of the American Water Resources Association*, 43(2), 482–498. <https://doi.org/10.1111/j.1752-1688.2007.00038.x>
- Wang, S.-Y. S., Yoon, J.-H., Becker, E., & Gillies, R. (2017). California from drought to deluge. *Nature Climate Change*, 7(7), 465. <https://doi.org/10.1038/nclimate3330>
- Welch, L.A., Allen, D.M., 2014. Hydraulic conductivity characteristics in mountains and implications for conceptualizing bedrock groundwater flow. *Hydrogeol J* 22, 1003–1026. <https://doi.org/10.1007/s10040-014-1121-5>

Wu, C., Liu, X., Lin, Z., Rhoades, A. M., Ullrich, P. A., Zarzycki, C. M., et al. (2017). Exploring a Variable-Resolution Approach for Simulating Regional Climate in the Rocky Mountain Region Using the VR-CESM. *Journal of Geophysical Research: Atmospheres*, 122(20), 10,939-10,965. <https://doi.org/10.1002/2017JD027008>

Zarzycki, C. M., Levy, M. N., Jablonowski, C., Overfelt, J. R., Taylor, M. A., and Ullrich, P. A. (2014). Aquaplanet Experiments Using CAM's Variable-Resolution Dynamical Core. *Journal of Climate* 27, 14, 5481-5503, <https://doi.org/10.1175/JCLI-D-14-00004.1>